Investigating the Impact of Conformational Molecular Engineering on the Crystal Packing of Cavity Forming Porphyrins

Keith J. Flanagan,[a] Brendan Twamley[b] and Mathias O. Senge[a]*

[a]School of Chemistry, SFI Tetrapyrrole Laboratory, Trinity Biomedical Sciences Institute, 152–160 Pearse Street, Trinity College Dublin, The University of Dublin, Dublin 2, Ireland

[b]School of Chemistry, Trinity College Dublin, The University of Dublin, Dublin 2, Ireland

KEYWORDS: Octaethylporphyrin, nonplanar porphyrins, halogen bonding, hydrogen bonding, X-ray crystallography, Click chemistry.

ABSTRACT. Herein we report the synthesis of 5,10,15,20-tetraaryl-(X)-substituted-2,3,7,8,12,13,17,18-octaethylporphyrins (OETArXPs) and a structural investigation of their solid-state properties *via* small molecule X-ray diffraction. A series of halogen (fluorine to iodine), nitrogenous (azido, cyano), alkyl (TMS-acetylene and acetylene) and chained (benzyloxy) porphyrins were chosen as the initial target molecules. Following this, a selection of tetravalent metal complexes [Cu(II), Ni(II) and Pd(II)] based on these porphyrins were synthesized to allow for an investigation of the effects of metal complexes on the structural properties of these highly substituted porphyrins. The size of the halogen atom affects the potential of intermolecular interactions and the resulting crystal packing in these 4-halo-OETArXP complexes. The fluorine series have an equal preference for alkyl or aryl

groups (*ortho*-hydrogen), the chlorine series favoring interactions between the alkyl groups, and the bromine appears to favor the aryl (*ortho*- and *meta*-hydrogens). This results in an extensive cupping pattern in the unit cell. For the 2,6-halo-OETArXP it was established that the change in position alters the types of the intermolecular contacts towards face-to-edge or face-to-face interactions and altering the packing patterns observed. Within the 4-benzyloxy-OETArXP series the meso-substituent favors interacting with the core of the porphyrin macrocycle. The 4-cyano-OETArXP is a suitable hydrogen-bond acceptor and resulted in an interesting Z-shape network. Additionally, it was highlighted that solvent effects play a much larger role in crystal packing than intermolecular/intramolecular interaction or metal(II) center substitution. This is accompanied by a study using both the azide- and acetylene-OETArXPs as a base molecule to allow for a quick one-step reaction for the generation of a variety of functional groups. Using a copper(I)-catalyzed azide-alkyne cycloaddition reaction we were able to append hydrogen bonding functionalities to the OETArXPs framework in high yields. The crystals packing of this work shows the potential to create selective and functional receptor sites based on free base porphyrins. However, in so far of analytical measurements indicate, the design such free base porphyrin through crystal engineering has not yet been realized. The variety of porphyrin packing arrangements herein indicates the need for further studies.

INTRODUCTION

Nonplanar porphyrins have grown into an molecule of high interest over the past few years in areas such as binding of small molecules as illustrated in a review by Kielmann and Senge[1] or as an organocatalyst as demonstrated by Roucan *et al.*[2] The key to their success in such areas is due to the accessibility of the inner core amine and imine moieties which are naturally shielded in their planar counterparts due to their conformation, Figure 1. This allows the core

of nonplanar porphyrins to freely interact with their environment, allowing for detailed investigations into core activity, as compared to the more traditional studies conducted on the peripheral and metal center effects. In nature, the conformation of tetrapyrroles is related to both the physiochemical properties and biological function. For example, chlorophyll a acts as an accessory and reaction center pigment in the photosynthesis of higher plants, bacteriochlorophyll a is found in the reaction centers and light-harvesting complexes of purple bacteria, and heme b which is involved in oxygen transport within the body.[3] The diverse application of these chemically similar compounds has long been prescribed to the macrocycle conformation within their specific protein structure.

Shielding   Non-shielding

—NH HN—   NH HN
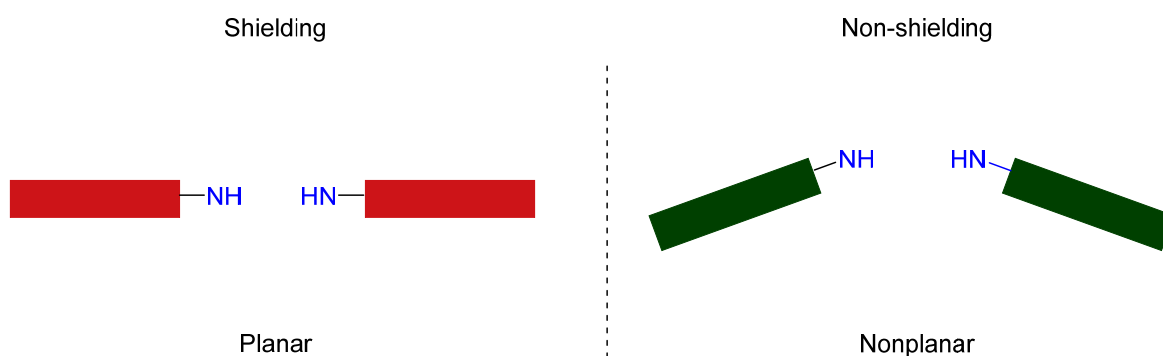
Planar   Nonplanar

Figure 1: Representation of the core shielding effect caused by planar porphyrins and how this is overcome in their nonplanar counterparts.

There are several ways to induce nonplanarity in a porphyrin;[4-5] the introduction of sterically demanding groups, metalation,[6-11] axial ligands,[12-13] reducing the porphyrin system,[14] alteration of the conjugated system,[14] *N*-substitution to the inner core nitrogen atoms,[15] cation radical formation,[16] "strapping" the macrocycle via covalent linkage,[17] or heteroatom substitution of the inner core nitrogen atoms.[18] For this publication, we have focused on increasing the steric hinderance through peripheral overcrowding of the porphyrin macrocycle. *peri*-Interactions usually cause the macrocycle to adopt a conformation in which less strain is applied, resulting in a nonplanar porphyrin. Increasing the number of

substitutions (mono- to dodecasubstituted) around the porphyrin periphery is typically accompanied by an increase in distortion.[19-20] The introduction of sterically demanding groups is a simple process that involves selecting an appropriate aldehyde (conventionally something bulky) and pyrrole (with functionalized β-carbons) and subsequently reacting them together using standard porphyrin condensation reactions.[21-23] This method is most useful for imparting aromatic moieties to the meso-position of the porphyrin ring. Other methods that have been reported are reacting β-functionalized porphyrins with an organolithium reagent, which is extremely useful for the synthesis of meso-alkyl substituted compounds,[24] *via* nucleophilic substitution such as S_NAr with aromatic thiols,[25] or the β-halogenation of the pyrrole units.[26] Other methods have been outlined in the highly substituted porphyrin chapter in the porphyrin handbook.[5] One of the main compound types which are used for the basis of studying nonplanar porphyrin is 5,10,15,20-tetraaryl-(X)-2,3,7,8,12,13,17,18-octaethylporphyin (OETArXP) and its derivatives. From this molecule, a large series of studies have been conducted, such as, investigating the role of hydrogen bonding in triggering spin-state crossing of cytochrome P450 catalysis using five-coordinate iron(III) octaethyltetraarylporphyrin chloride derivatives,[27] use as a catalyst to produce *N*-aryl-2-vinylaziridines,[28] examining d-π exchange and charge transfer,[29] metal-organic frameworks,[30] or examining the impact of substituents and steric effects of porphyrins among other areas.[19, 31] However, the breath of compounds used in these studies is rather limited. Considering only the free base analogs (as most of these studies use their metal derivatives) there are only 19 known OETArXP compounds. These are listed in Figure S1. Additionally, the synthesis of these compounds is strictly around the traditional condensation reactions and relies on any modifying the pyrrole subunit prior to the condensation reaction to impart functionality as seen in the works of Liu *et al*.[30] This results in a low yields, complicated synthesis, and a gap in the current literature for a convenient porphyrin precursor which could be easily modified

to generate a large variety of derivatives. The first part of this publication will focus on increasing the current library of OETArXP compounds and establishing two systems which would allow for a porphyrin base molecule to be used as a precursor for further functionalization.

The second part of this publication will be centered around a structural discussion of OETArXP compounds obtained as part of this publication. Previously it has been determined that out-of-plane macrocycle distortion, together with the orientation of the ethyl groups leads to the formation of binding cavities on both sides of the porphyrin.[5] This results in frequent incorporation of solvent molecules in the crystal structure due to their saddle shape, forming tunnel-like structures. Considering this, OETArXP systems may make for an ideal candidate for non-covalent organic frameworks; however, to date, no report on this topic exists. The concept of crystal engineering of porphyrins has been around for over three decades with Byrn *et al.* purposing the idea that the highly ordered 'porous' structure of porphyrin clathrates can be used as a form of 'porphyrin sponge'.[32] In this regard, a tetraphenylporphyrin host was reported to trap a variety of guests within its crystal using strictly hydrogen-bonding and van der Waals forces. Since then, crystal engineering of porphyrins has focused on the use of planar porphyrins with a variety of non-covalent interactions such as hydrogen-bonds, metal coordination and halogen-bonding interactions.[32-44] Goldberg and co-workers have widely published on the use of 5,10,15,20-tetraarylporphyrins bearing either a carboxylic acid, pyridine or amine functionality forming non-covalent systems through hydrogen-bonds and metal coordination.[33-37, 39, 41-44] These complexes have been reported to be of use in a range of areas in material sciences, such as molecular sieves, due to the formation of a three-dimensional lattice in which more than 50% of the crystal volume consisted of open straight channels.[36-37] Other notable reports are those by Titi *et al.* on the self-assembly of tetraarylporphyrins through halogen-bonding forming a

chiral architecture based on C–I···N and C–I···π interactions,[38] or the works reported by Patra *et al.* who utilized the coordination of tin to carboxylic acids to form a supramolecular organized network by exploiting cooperative hydrogen-bonding with axial bound ligands.[45]

However, with all the advances made in the crystal engineering of planar porphyrins, investigation of their nonplanar counterparts has been practically unexplored with regards to non-covalent interactions and their applications in the formation of molecular cages. The main benefit of this is that with higher degrees of distortion, the meso-substituted groups themselves are forced further from the plane of the porphyrin ring. This allows for the potential of interactions to take place between co-facial molecules. This application has been touched on, e.g., by Gilday *et al.* in which the planar 5,10,15,20-tetrakis(3-(azidomethyl)phenyl)porphyrin was 'strapped' with tetra(prop-2-yn-1-yl) benzene-1,2,4,5-tetracarboxylate through a copper(I)-catalyzed azide-alkyne cycloaddition (CuAAC).[46] The authors carried out successful anion binding studies which showed a 1:1 receptor to anion-binding stoichiometry and a clearly visible color change depending on the anion.

The structural properties of porphyrins have attracted significant interest since they were first described, and a range of nonplanar porphyrin structures were published over the years.[7, 10, 13, 20, 24-25, 47-52] However, in terms of crystal engineering, the emphasis to date has mainly focused on planar porphyrin species, such as the studies done by Goldberg and co-workers.[32-45, 53] With the benefits afforded to nonplanar porphyrins, the time to discuss their potential in such fields is apparent. Herein we are aiming to investigate the noncovalent interactions between nonplanar porphyrin scaffold in an attempt to generate a molecular cage through intermolecular interactions. The main areas we hope to analysis during this project are change in substituent groups and position, affects between freebase and metal centers, and the inclusion of solvent molecules. With this in mind, we established a library of several of new

OETArXP compounds through traditional condensation reactions or CuAAC to investigate the impact on conformational molecular engineering on the crystal packing of nonplanar porphyrins through small molecule X-ray diffraction.

EXPERIMENTAL SECTION

All commercial chemicals used were of analytical grade and supplied by Sigma Aldrich, Frontier Scientific, Inc., Tokyo Chemical Company and Acros chemicals and used without further purification unless otherwise stated. Anhydrous CH_2Cl_2 (for porphyrin synthesis) was obtained *via* distillation over phosphorus pentoxide. All microwave reactions were run on a Biotage Initiator+ without supplemental pressure. Flash column chromatography was carried out using Fluka Silica Gel 60 (230-400 mesh; Merck). Mobile phases are described as (v/v) if isocratic, or % gradients. Analytical thin-layer chromatography (TLC) was performed using silica gel 60 (fluorescence indicator F_{254}, precoated sheets, 0.2 mm thick, 20 cm × 20 cm; Merck) and visualized by UV irradiation. Melting points are uncorrected and were measured with a Stuart SP-10 melting point apparatus. A Bruker Advance III 400 MHz, a Bruker DPX400 400 MHz and an Agilent 400 spectrometer were employed for ^1H (400.13 MHz), ^{19}F (376.60 MHz) and ^{13}C (100.61 MHz) NMR spectra and a Bruker Ultrashield 600 spectrometer was employed for ^1H (600.13 MHz), ^{13}C (150.90 MHz) NMR spectra. All NMR experiments were performed at room temperature unless otherwise stated. Resonances δ, are given in ppm units and referenced to the deuterium peak in the NMR solvent of $CDCl_3$ (δ_H = 7.26 ppm, δ_C = 77.0 ppm). The assignment of the signals was confirmed by selective 2D spectra (COSY and HSQC). Mass spectrometry analysis was performed with a Q-Tof Premier Waters MALDI quadrupole time-of-flight (Q-TOF) mass spectrometer equipped with Z-spray electrospray ionization (ESI) and matrix-assisted laser desorption ionization (MALDI) sources either in a positive or negative mode with DCTB (*trans*-2-[3-(4-*tert*-

butylphenyl)-2-methyl-2-propenylidene]malononitrile) as the matrix. ESI mass spectra were acquired in positive or negative modes as required, using a Micromass time of flight mass spectrometer (TOF) interfaced to a Waters 2960 HPLC, or a Bruker microTOF-Q III spectrometer interfaced to a Dionex UltiMate 3000 LC. APCI experiments were performed on a Bruker microTOF-Q III spectrometer interfaced to a Dionex UltiMate 3000 LC. Photophysical measurements were carried out in CH_2Cl_2 as a solvent. UV-visible absorption measurements were performed using a Shimadzu MultiSpec-1501.

General Procedure A: The Synthesis of Free Base OETArXPs. Dry CH_2Cl_2 (1 L), 3,4-diethylpyrrole (1 g, 8.12 mmol, 1 eq.) and aldehyde (8.12 mmol, 1 eq.) were placed in a 2 L round-bottom flask and stirred for 10 minutes. $BF_3 \cdot Et_2O$ (0.10 mL, 0.81 mmol, 0.1 eq.) was added to the mixture and left to stir for 18 h at room temperature. DDQ (1.84 g, 8.12 mmol, 1 eq.) was added and the solution was stirred for 1 h. The reaction was quenched with TEA (0.11 mL, 0.81 mmol, 0.1 eq.). The solvent was evaporated to dryness and the residue taken up in CH_2Cl_2. The mixture was ultrasonicated for 2 min and then filtered through a plug of silica, washing with 1% MeOH in CH_2Cl_2. The eluted porphyrin fractions were evaporated to dryness and purified by silica gel chromatography using *n*-hexane:EtOAc (4:6) and dried in vacuo to yield the compound as green flakes.

General Procedure B: The Synthesis of Nickel(II) OETArXPs. The free base porphyrin (1 eq.) was dissolved in toluene (5 mL) and heated to reflux with nickel(II) acetylacetonate (5 eq.) for 18 hours. The reaction was monitored by TLC control and the solvent removed under reduced pressure. The residue was dissolved in CH_2Cl_2 and the mixture filtered through silica gel, eluting with CH_2Cl_2. The solvent was removed under reduced pressure and the product dried under high vacuum. The resulting solid was dissolved in a minimal amount of CH_2Cl_2 and layered with MeOH for recrystallization, resulting in purple crystals.

General Procedure C: The Synthesis of Copper(II) OETArXPs. The free base porphyrin (1 eq.) was dissolved in toluene (5 mL) and heated to reflux with copper(II) acetate (5 eq.) for 18 hours. The reaction was monitored by TLC control and the solvent removed under reduced pressure. The residue was dissolved in CH_2Cl_2 and the mixture filtered through silica gel, eluting with CH_2Cl_2. The solvent was removed under reduced pressure and the product dried in high vacuum. The resulting solid was dissolved in a minimal amount of CH_2Cl_2 and layered with MeOH for recrystallization, resulting in purple crystals.

General Procedure D: The Synthesis of Palladium(II) OETArXPs. The free base porphyrin (1 eq.) was dissolved in toluene (5 mL) and heated to reflux with palladium(II) acetate (5 eq.) for 18 hours. The reaction was monitored by TLC control and the solvent removed under reduced pressure. The residue was dissolved in CH_2Cl_2 and the mixture filtered through silica gel, eluting with CH_2Cl_2. The solvent was removed under reduced pressure and the product dried under high vacuum. The resulting solid was dissolved in a minimal amount of CH_2Cl_2 and layered with MeOH for recrystallization, resulting in purple crystals.

General Procedure E: The Synthesis of 'Click' OETArXPs. The porphyrin **77**, azide coupling partner, sodium ascorbate (0.4 eq.) and $Cu(OAc)_2$ (0.4 eq.) were dissolved in THF (5 mL) and heated in a microwave reactor for 20 minutes. The solvent was removed under reduced pressure. The residue was dissolved in CH_2Cl_2 and the mixture filtered through silica gel, eluting with CH_2Cl_2:EtOAc (1:1). The solvent was removed under reduced pressure and the product dried under high vacuum. The resulting solid was dissolved in a minimal amount of CH_2Cl_2 and layered with MeOH for recrystallization, resulting in purple crystals.

X-ray Crystallography. Crystals were grown following the protocol developed by Hope by dissolving the compounds in either CH_2Cl_2, a CH_2Cl_2/MeOH mixture, or $CDCl_3$ and layering

with a second solvent (MeOH or hexane) for liquid diffusion or allowing for slow evaporate over time.[54] Single crystal X-ray diffraction data for all compounds were collected on a Bruker APEX 2 DUO CCD diffractometer by using graphite-monochromated Mo K$_\alpha$ ($\lambda = 0.71073$ Å) radiation and Incoatec IμS Cu K$_\alpha$ ($\lambda = 1.54178$ Å) radiation. Crystals were mounted on a MiTeGen MicroMount and collected at 100(2) K by using an Oxford Cryosystems Cobra low-temperature device. Data were collected by using omega and phi scans and were corrected for Lorentz and polarization effects by using the APEX software suite.[55-57] Using Olex2, the structure was solved with the XT structure solution program, using the intrinsic phasing solution method and refined against │F2│ with XL using least squares minimization.[58-59] Hydrogen atoms were generally placed in geometrically calculated positions and refined using a riding model. Details of data refinements can be found in Table S1-S4. All images were prepared by using Olex2.[58] A detailed discussion on data modelling is covered in the supporting information (page 68).

Normal-coordinate Structural Decomposition (NSD) Analysis. The theoretical background and development of this method have been described by Shelnutt and co-workers.[3, 60-62] NSD is a conceptually simple method that employs the decomposition of the conformation of the macrocycle by a basis set composed of its various normal modes of vibration, affording clear separation of the contributing distortions to the macrocycle conformation in a quantitative fashion. For calculations, we used the NSD engine program as provided by Shelnutt.[63]

Hirschfeld Surface Analysis. The Hirschfeld surface analysis and 2D fingerprint plots were drawn using the program CrystalExplorer17 (version 17.5) by importing the CIF files for the corresponding crystal structures.[64] The quantifying and decoding of the intermolecular contacts in the crystal packing is visualized using d_{norm} (normalized contact distance) and 2D

fingerprint plots, respectively. The dark-red spots on the d_{norm} surface arise as a result of short interatomic contacts, while the other intermolecular interactions appear as light-red spots. d_i (inside) and d_e (outside) represent the distances to the Hirshfeld surface from the nuclei, with respect to the relative van der Waals radii. The proportional contribution of the contacts over the surface is visualized by the color gradient (blue to red) in the fingerprint plots. The overall surface cover (given in %) was tabulated using Microsoft Excel for hydrogen···hydrogen (H···H), X···hydrogen (X···H, were X is either a halogen or oxygen atom), carbon···carbon (C···C), nitrogen···hydrogen (N···H), metal(II)···hydrogen (M···H) and X···X (were X is either a halogen or oxygen atom) atoms. For a more detailed description on how to use fingerprint plots please see the original work by Spackman and Jayatilaka.[65]

RESULTS AND DISCUSSION

For this project, several groups of porphyrins were chosen for their potential to form non-covalent interactions and were achieved through a traditional condensation reaction for 5,10,15,20-tetraarylsubstituted porphyrins resulting in compounds **13–23** (Scheme 1).[66] A series of compounds **13–18** bearing a halogen in either the *ortho-* or *para-*position of the meso-aryl residue were prepared to examine the effects of halogen functionalization on the interaction profile of OETArXP. The synthesis of compounds **15** and **18** were previously reported by Schindler *et al.* and Hoshino *et al.*, respectively.[67-68] Compound **15** was included as most of its metal counterparts have not been previously published and the literature for compound **18** does not contain a detailed experimental. Two benzyloxy chained porphyrins, 4-benzyloxyphenyl-OETArXP (**20**), and 3,4-dibenzyloxyphenyl-OETArXP (**21**), were chosen as they contain bulky groups and can be used to investigate steric effects. The 4-cyanophenyl-OETArXP (**22**) was included as cyano groups, due to their electron rich nature
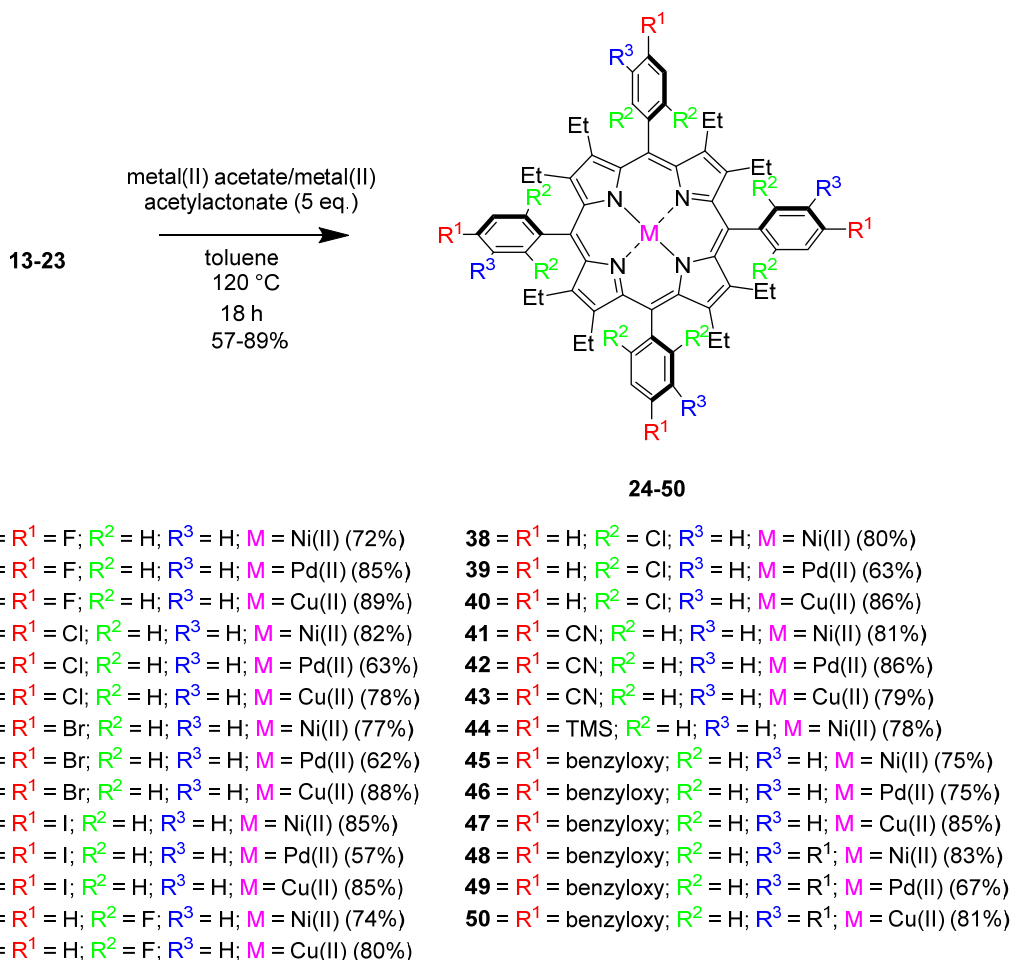
and 2-D connections, provide an interesting tecton for the synthesis of non-covalent networks.[44] Such moieties have been used as a weak hydrogen-bond acceptor in supramolecular arrays and as suitable halogen-bond acceptors. Goldberg and co-workers have utilized this specific moiety link porphyrin systems through non-covalent interactions.[44] Finally, compounds 4-azidophenyl-OETArXP (**23**) 4-((trimethylsilyl)ethynyl)phenyl-OETArXP (**19**) were synthesized as a precursor for larger porphyrin arrays. To expand the library of OETArXP compounds available for it was decided to include the metal(II) derivatives with either nickel(II), copper(II), or palladium(II). The synthesis of the metal(II) derivatives of OETArXP was achieved by the addition of metal(II) acetate or metal(II) acetylacetonate to a solution of the free base porphyrin (**13–23**) in toluene and heating to 120 °C for 18 h to yield compounds **24–50** (Scheme 2).[69] The synthesis of compound **30** has been previously reported by Schindler *et al*.[67]

Scheme 1: Free base OETArXP synthesized.
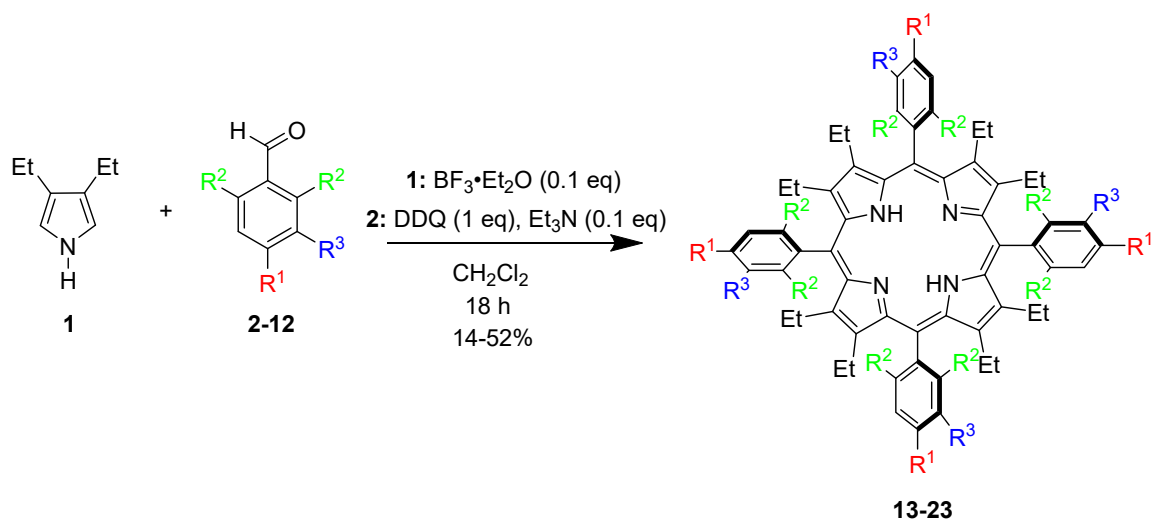
$2 = R^1 = F; R^2 = H; R^3 = H$

$3 = R^1 = Cl; R^2 = H; R^3 = H$

$4 = R^1 = Br; R^2 = H; R^3 = H$

$5 = R^1 = I; R^2 = H; R^3 = H$

$6 = R^1 = H; R^2 = F; R^3 = H$

$7 = R^1 = H; R^2 = Cl; R^3 = H$

$8 = R^1 = TMS\ acetylene; R^2 = H; R^3 = H$

$9 = R^1 = benzyloxy; R^2 = H; R^3 = H$

$10 = R^1 = benzyloxy; R^2 = H; R^3 = benzyloxy$

$11 = R^1 = CN; R^2 = H; R^3 = H$

$12 = R^1 = N_3; R^2 = H; R^3 = H$

$13 = R^1 = F; R^2 = H; R^3 = H\ (30\%)$

$14 = R^1 = Cl; R^2 = H; R^3 = H\ (28\%)$

$15 = R^1 = Br; R^2 = H; R^3 = H\ (33\%)$

$16 = R^1 = I; R^2 = H; R^3 = H\ (14\%)$

$17 = R^1 = H; R^2 = F; R^3 = H\ (20\%)$

$18 = R^1 = H; R^2 = Cl; R^3 = H\ (17\%)$

$19 = R^1 = TMS\ acetylene; R^2 = H; R^3 = H\ (52\%)$

$20 = R^1 = benzyloxy; R^2 = H; R^3 = H\ (37\%)$

$21 = R^1 = benzyloxy; R^2 = H; R^3 = benzyloxy\ (28\%)$

$22 = R^1 = CN; R^2 = H; R^3 = H\ (29\%)$

$23 = R^1 = N_3; R^2 = H; R^3 = H\ (21\%)$

Scheme 2: Synthesis of metal(II) OETArXP compounds.

24 = R^1 = F; R^2 = H; R^3 = H; M = Ni(II) (72%)
25 = R^1 = F; R^2 = H; R^3 = H; M = Pd(II) (85%)
26 = R^1 = F; R^2 = H; R^3 = H; M = Cu(II) (89%)
27 = R^1 = Cl; R^2 = H; R^3 = H; M = Ni(II) (82%)
28 = R^1 = Cl; R^2 = H; R^3 = H; M = Pd(II) (63%)
29 = R^1 = Cl; R^2 = H; R^3 = H; M = Cu(II) (78%)
30 = R^1 = Br; R^2 = H; R^3 = H; M = Ni(II) (77%)
31 = R^1 = Br; R^2 = H; R^3 = H; M = Pd(II) (62%)
32 = R^1 = Br; R^2 = H; R^3 = H; M = Cu(II) (88%)
33 = R^1 = I; R^2 = H; R^3 = H; M = Ni(II) (85%)
34 = R^1 = I; R^2 = H; R^3 = H; M = Pd(II) (57%)
35 = R^1 = I; R^2 = H; R^3 = H; M = Cu(II) (85%)
36 = R^1 = H; R^2 = F; R^3 = H; M = Ni(II) (74%)
37 = R^1 = H; R^2 = F; R^3 = H; M = Cu(II) (80%)

38 = R^1 = H; R^2 = Cl; R^3 = H; M = Ni(II) (80%)
39 = R^1 = H; R^2 = Cl; R^3 = H; M = Pd(II) (63%)
40 = R^1 = H; R^2 = Cl; R^3 = H; M = Cu(II) (86%)
41 = R^1 = CN; R^2 = H; R^3 = H; M = Ni(II) (81%)
42 = R^1 = CN; R^2 = H; R^3 = H; M = Pd(II) (86%)
43 = R^1 = CN; R^2 = H; R^3 = H; M = Cu(II) (79%)
44 = R^1 = TMS; R^2 = H; R^3 = H; M = Ni(II) (78%)
45 = R^1 = benzyloxy; R^2 = H; R^3 = H; M = Ni(II) (75%)
46 = R^1 = benzyloxy; R^2 = H; R^3 = H; M = Pd(II) (75%)
47 = R^1 = benzyloxy; R^2 = H; R^3 = H; M = Cu(II) (85%)
48 = R^1 = benzyloxy; R^2 = H; R^3 = R^1; M = Ni(II) (83%)
49 = R^1 = benzyloxy; R^2 = H; R^3 = R^1; M = Pd(II) (67%)
50 = R^1 = benzyloxy; R^2 = H; R^3 = R^1; M = Cu(II) (81%)

Arm-extended porphyrins. One of the initial points was to establish a porphyrin system which could be used as a simple starting material for further functionalization. It was first considered that either the bromine (**15**) or iodine (**16**) could be used in a palladium-catalyzed cross-coupling reaction; however, initial reactions quickly determined that this was not possible. This is either due to the steric influence of the ethyl groups on the periphery of the ring or a combination of steric and electronic of the nonplanar macrocycle, causing the 4-bromophenyl substituent to become electron deficient and unfavorable to palladium catalyzed cross-couplings. To circumvent this issue, we decided to move towards using a copper(I)-catalyzed azide-alkyne cycloaddition (CuAAC).[70] This could be achieved by using the 4-

azidophenyl-OETArXP (**23**) or nickel(II) 4-ethynylphenyl-OETArXP (**51**) which was obtained by deprotecting compound **44** using TBAF (Scheme 3).
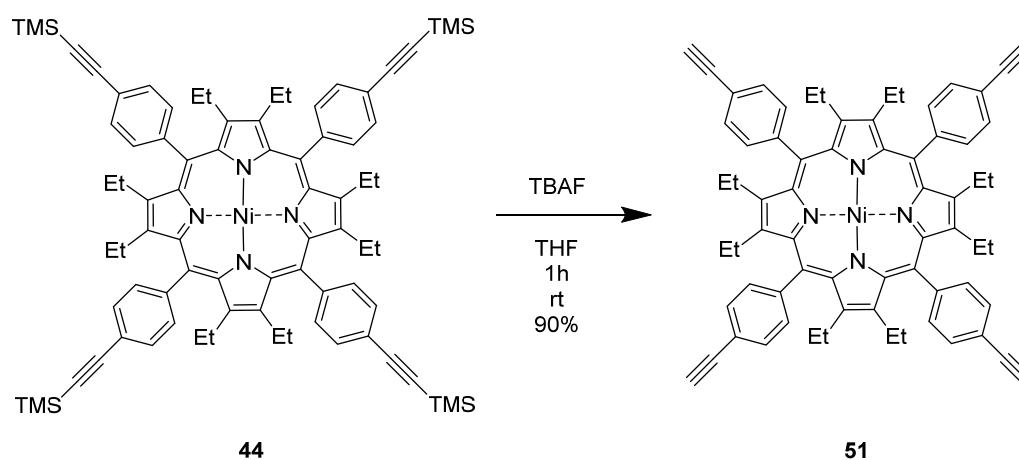

Scheme 3: Deprotection of compound **44**.

A series of azide compounds were needed to couple with compound **51**. For this, a procedure outlined by Grimes *et al.*, in which the boronic acid precursor was stirred in the presence of NaN$_3$ for three hours in MeOH was chosen.[71] This resulted in the synthesis of **53**, **55**, **57**, **59**, and **61** (Scheme 4). Following this, the arm-extended porphyrins, compounds **62–66**, were synthesized by CuAAC using the appropriate four-fold excess of the azide in the presence of sodium ascorbate and Cu(OAc)$_2$ using a microwave reactor (Scheme 5). It was noted that these reactions proceeded in relatively high yields over a short reaction time. This indicates the versatility of this reaction to accommodate a variety of functional groups by a simple one-step reaction. The only limitation to this reaction is the access to suitable azide coupling partners.
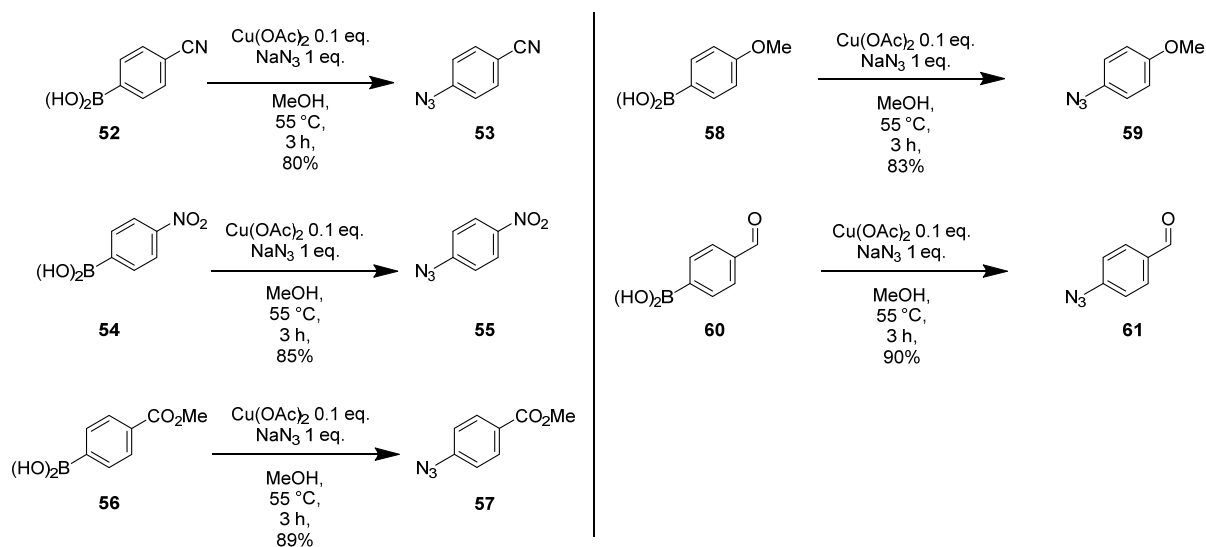
**Scheme 4:** Synthesis of azide coupling partners for arm-extended porphyrins.
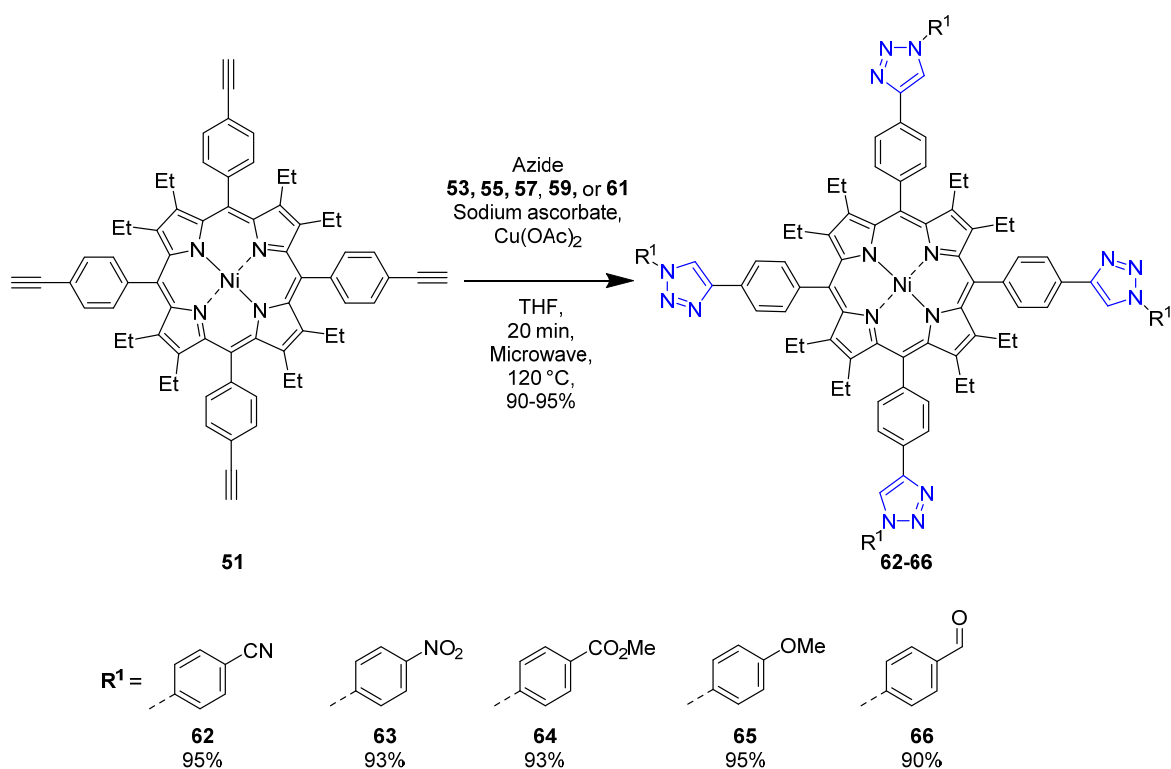
Scheme 5: Synthesis of arm-extended porphyrins from acetylene porphyrin (**51**) (acetylene-click process).

The benefit and versatility of the acetylene-click process (Scheme 5) are evident; however, it was felt prudent to investigate the inverse reaction. To do this, we chose to react methyl 4-

ethynylbenzoate with porphyrin **23** using the same conditions used in Scheme 5 (Scheme 6). Following washing the compounds with a dilute acid solution to remove the copper insertion, compound **67** was achieved in a 53% yield, which is considerably lower than that for compounds **62–66**. While the yield is lower, taking into consideration that this process is a one-step reaction from the free base porphyrin, while the products shown in Scheme 5 are a three-step reaction process from the free base porphyrin **19**. This reaction demonstrates the versatility of using alternate porphyrin scaffolds to achieve compounds with almost identical functionality.
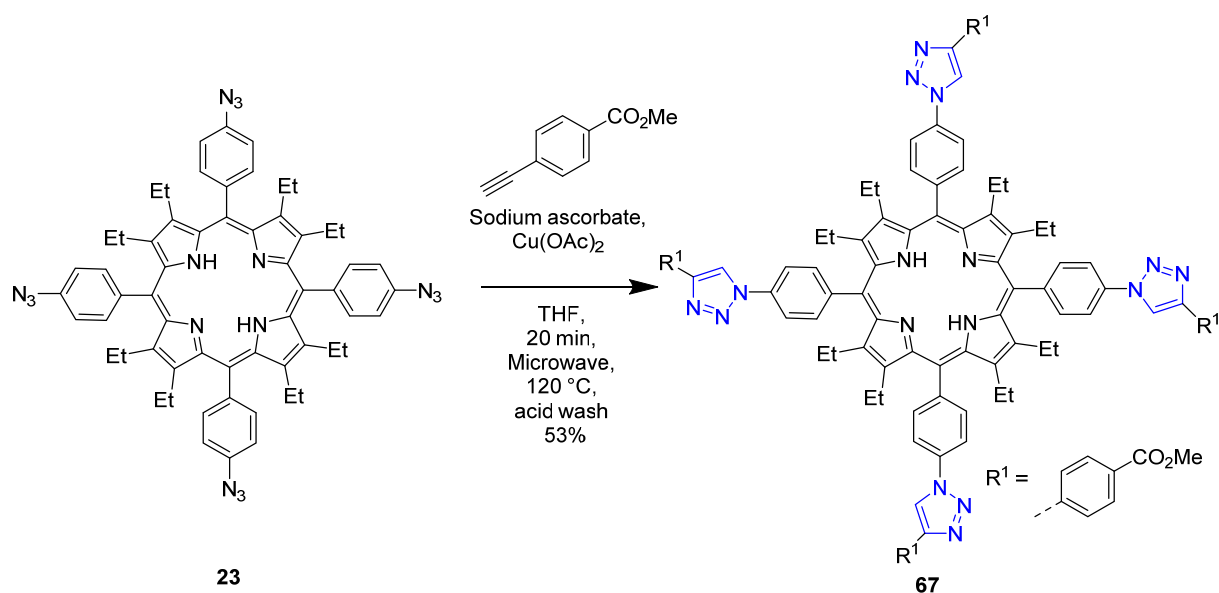
Scheme 6: Synthesis of arm-extended porphyrins from azide porphyrin (**23**) (azide-click process).

Both the acetylene-click process (Scheme 5) and the azide-click process (Scheme 6) show a potential to use OETArXP as a scaffold for large nonplanar porphyrin arrays. As is noted during the synthesis of compound **67**, the free base form of each compound can be easily achieved by simply acid wash, due to a weak association of the central metal ion. With this in mind, these compounds would be available to be used in their free base forms or

accommodate any desirable metal ion. Such compounds could provide the basis for a variety of studies such as the using compound **66** being incorporated into chitosan hydrogel or studying organocatalyst as demonstrated by Roucan *et al.*[2]

Structure of OETArXP Compounds. Crystal packing studies of highly substituted nonplanar porphyrins is a well-established field.[4, 7, 10, 13, 20, 24-25, 47-52, 72] However, detailed studies in the crystal engineering of nonplanar porphyrins have not been conducted to date. An investigation into the intermolecular and crystal packing effects of both halogenated and non-halogenated substituted derivatives was undertaken on the synthesized OETArXP (**13–23**) and the metalloporphyrin derivatives (**24–50**). Single crystals of compounds **13**–**23** proved difficult to obtain with only the free base derivative **18A** (where 'A' denotes the CDCl$_3$ solvated versions) giving crystals of reasonable quality. From the metalloporphyrin derivatives (**24–50**) 12 crystals of sufficient quality for X-ray diffraction were obtained, **24**, **25**, **27**, **30B**, **32**, **36**, **38A**, **39**, **40**, **40A**, **41**, and **45** (where 'A' denotes the CDCl$_3$ solvated versions and 'B' denotes the CH$_2$Cl$_2$ solvated version).

It can be seen from the crystal structures (Figure S2-S14) that the porphyrin rings are severely distorted. The tilt angles of the pyrrole rings are larger compared to planar porphyrins which result in a higher degree of atom displacement from the 24-atom least squares plane. The phenyl groups exhibit a similar tilt angle from the 24-atom least-squares plane of 38–59˚ with the largest deviation associated with compound **39** (47.1–59.0°). The average N–metal bonds are comparable with other nonplanar porphyrins found in the literature for both Cu(II) and Ni(II) complexes, Table 1.[20, 73]

The conformational analysis of porphyrins requires the determination of specific geometrical parameters complemented by a visual description. The simplest depiction of this is the displacement of atoms from the 24-atom least-squares plane as a skeletal deviation plot

(Figure S14). It should be noted that atoms, which deviate the most from the 24-atom least-squares plane, are the β-carbons (Figure S15-S16). The β-carbons are featured in an alternating pattern above and below the 24-atom macrocycle least-squares plane and the nitrogen atoms are all close to the mean plane. This results in a saddle type porphyrin structure. Due to the aryl groups present, steric crowding favors this conformation which can be clearly seen by looking at the NSD plots, Figure S17. This saddle type distortion is also evident in the molecular structures shown in Figure S2-S14. In comparison to previous studies conducted within the group on unsymmetrical decasubstituted OEP structures, the porphyrin structure presented here show similar overall out-of-plane contributions for saddle distorted porphyrins, with regards to the 24-atom least-squares plane.[52]

There are two other features of these compounds that are common to all of these structures included herein. These are the effects that metals and solvents have on the crystal packing within this series. While the structures will be discussed in individual detail, it feels prudent to highlight these effects to avoid needless repetition. As has previously been observed in the structure of 2,3,7,8,12,13,17,18-octaethyl-5,10,15,20-tetraphenylporphyrin derivatives and their metal counterparts that the size of the metal ion influences the distortion porphyrin macrocycle as larger metal ion lead to a less distorted conformation.[4, 74] With this in mind we considered to see if this influence on distortion was sufficient to alter the packing patterns observed for the OETArXP compounds herein. It was noted that changing the metal(II) center has only marginal effects on the structure of the porphyrin macrocycle. Considering Table 1, the most obvious change is the N–metal bond lengths are increased depending on the size of the metal in the porphyrin core. There are also minor changes to the pyrrole tilt angle (decreasing) and phenyl ring tilt angles (increasing) by around ~1–2° with increasing metal ion size. However, with these minor structural changes there is no observable difference when examining the crystal packing. This is seen clearly in the crystal packing of the

structures of **24** and **25** (Figure 2). Both compounds are structurally similar with no solvent molecules presented. The only difference between the structures is the metal(II) center [Ni(II) (**24**) and Pd(II) (**25**)] and as such, both compounds result in almost identical packing patterns.
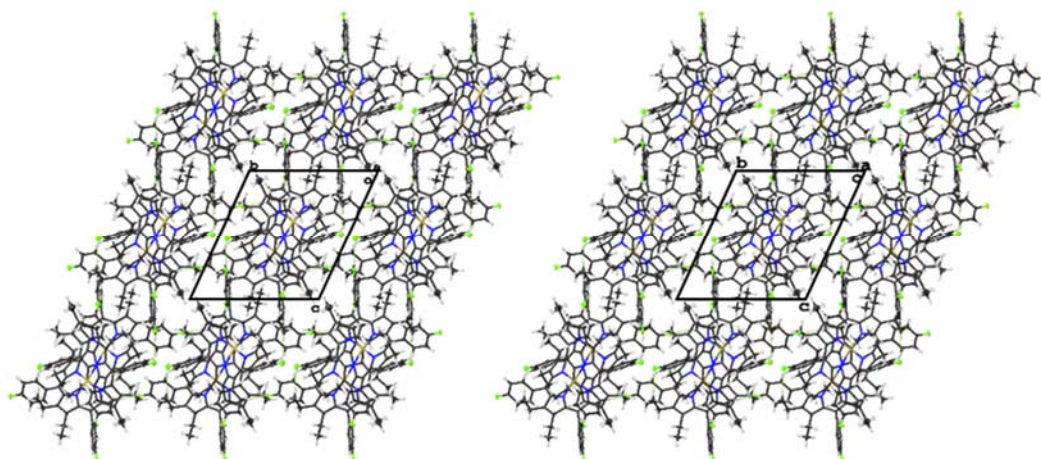
Figure 2: Crystal packing image (looking down the *a*-axis) of compounds **24** (left) and **25** (right) showing the similarities between the crystal packing of two alternate metal complexes of OETArXP structures. Thermal displacement is given at 50% probability.

Solvent inclusion has much more of an effect on the porphyrin structures. This is clearly seen in the structure of **40** and **40A** in which the inclusion of solvent results in a small decrease in the N–Metal bond lengths. The phenyl ring tilt angles show a ~7° decrease and pyrrole tilt angles show a ~4° increase as a result of including the solvent. However, the most obvious difference is seen in the crystal packing of **40** (Figure 3a) and **40A** (Figure 3b), in which the packing pattern alters significantly from the tightly stacked structure of **40** to the much looser pattern on **40A** in which the porphyrin layers are separated by a solvent channel in an ABAB type pattern (Figure 3). This is further compounded when looking the crystal packing of **32** (Figure 3c) and **30B** (Figure 3d) where the tightly cupped pattern is of **32** is more spaced out in **30B** due to the inclusion of a DCM molecule between the layers of porphyrin molecules to form an ABBA type pattern. As shown by comparing **24** and **25** the choice of metal(II) center

does not affect the packing to any significant degree, therefore the differences seen between **32** and **30B** are a direct result of the included solvent molecule. The interesting question at this point is the fact that two solvents result in two alternate packing patterns, however, the effect that the substituent type and pattern has in connection to solvent inclusion is still to be determined. These types of inclusion complexes are reminiscent to the porphyrin sponges reported by Byrn *et al*. which opens an avenue for further study.[32]
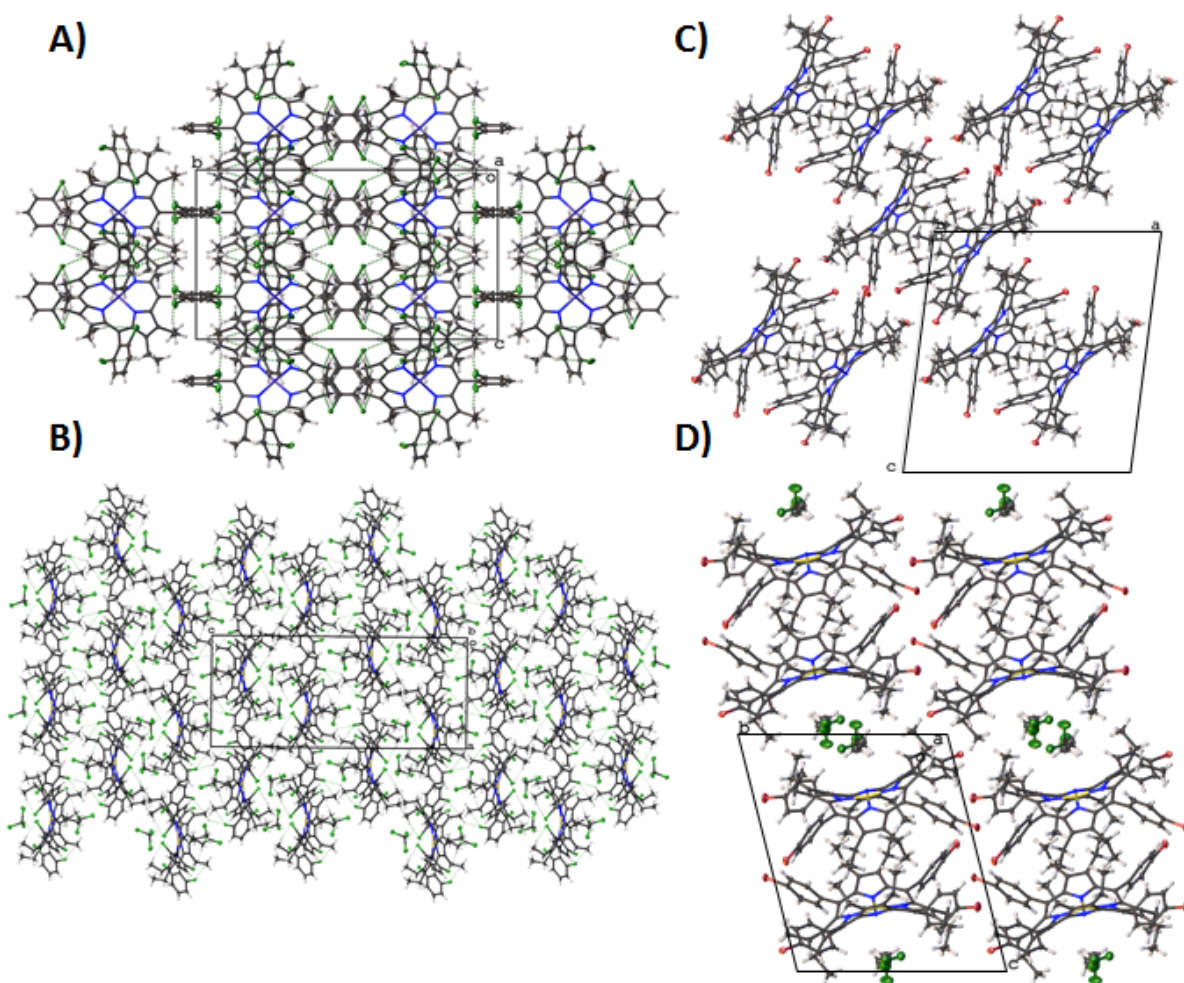
Figure 3: Crystal packing image of compounds **40** (A), **40A** (B), **32** (C), and **30B** (D) showing the differences caused by the inclusion of solvent to OETArXP structures. Thermal displacement is given at 50% probability.

Table 1: Selected geometrical parameters of OETArXP crystal structures.

Compound	18A	24	25	27[i]	27[ii]	30B	32	36[i]
Pyrrole tilt angle (°)								
N21	21.8(3)	25.2(4)	25.9(7)	30.5(7)	29.7(7)	27.3(7)	32.8(11)	24.7(6)
N22	30.5(3)	26.4(4)	24.6(7)	26.7(6)	26.6(6)	32.3(8)	26.1(11)	27.0(6)
N23	31.2(3)	26.5(4)	23.9(6)	31.5(6)	30.5(6)	27.4(8)	30.1(11)	25.5(6)
N24	30.8(3)	25.2(4)	26.0(6)	25.5(7)	28.1(7)	30.1(8)	24.9(11)	27.6(6)
Phenyl ring tilt angle (°)								
C5	52.3(3)	54.6(4)	56.0(6)	45.6(11)	45.0(7)	38.5(8)	40.8(11)	53.7(6)
C10	43.5(3)	53.7(4)	52.7(7)	40.1(6)	42.0(6)	38.7(8)	46.6(10)	45.9(6)
C15	42.0(3)	49.7(4)	50.2(7)	42.7(6)	40.4(6)	56.8(6)	46.5(10)	47.3(6)
C20	47.7(3)	51.6(4)	53.4(6)	46.4(6)	46.9(6)	48.7(8)	41.6(10)	47.2(7)
N-Metal bond length (Å)								
N21	n/a	1.913 (1)	2.008(2)	1.923(2)	1.917(2)	1.896(2)	1.975(4)	1.908(2)
N22	n/a	1.917 (1)	2.007(2)	1.903(2)	1.904(2)	1.914(3)	1.970(4)	1.923(2)
N23	n/a	1.927 (1)	2.013(2)	1.914(2)	1.912(2)	1.892(2)	1.982(4)	1.912(2)
N24	n/a	1.923 (1)	2.020(2)	1.903(2)	1.905(2)	1.917(2)	1.961(3)	1.923(2)

[a] bond length or angle generated and calculated over symmetry.

Table 1 (continued): Selected geometrical parameters of OETArXP crystal structures.

Compound	36[ii]	38A	39	40	40A	41	45[i]	45[ii]
Pyrrole tilt angle (°)								
N21	28.6(6)	28.6(5)	25.1(7)	24.2(6)	27.4(13)	31.9(4)	37.7(13)	28.2(12)
N22	28.8(6)	28.8(10)	23.5(8)	25.6(6)	26.9(13)	31.8(6)	28.4(12)	32.3(12)
N23	29.3(6)	28.1(10)	23.5(8)[a]	25.6(6)	29.0(12)	31.9(4)	29.8(13)	24.2(16)
N24	29.4(6)	27.6(10)	25.1(7)[a]	24.2(6)	29.1(12)	30.1(6)	29.1(12)	29.5(12)
Phenyl ring tilt angle (°)								
C5	47.2(6)	44.2(10)	59.0(8)	58.2(6)	46.6(12)	38.2(4)	36.7(11)	42.7(2)
C10	53.0(6)	44.3(10)	51.0(10)	46.9(8)	47.9(12)	38.2(4)[a]	46.5(16)	50.1(12)
C15	48.0(7)	46.0(10)	59.0(8)[a]	58.2(6)[a]	44.6(12)	40.0(4)[a]	42.9(12)	53.8(13)
C20	49.9(7)	47.4(10)	47.1(10)	49.7(9)	45.0(13)	40.0(4)	34.7(2)	42.9(11)
N-Metal bond length (Å)								
N21	1.902(2)	1.905(3)	2.010(2)	1.977(17)	1.967(4)	1.907(13)	1.911(4)	1.908(3)
N22	1.886(2)	1.904(3)	2.014(2)	1.973(17)	1.964(4)	1.903(18)	1.898(4)	1.919(3)
N23	1.902(2)	1.902(3)	2.010(2)	1.973(17)	1.963(4)	1.907(13)	1.902(4)	1.907(4)
N24	1.903(2)	1.896(3)	2.014(2)	1.977(17)	1.960(4)	1.902(18)	1.901(4)	1.903(3)

[a] bond length or angle generated and calculated over symmetry.

Increasing the Size of the Halogen. As outlined previously the main objective of this project was the crystal engineering of highly substituted porphyrin species for the investigation of the influence of substituent type and pattern on crystal packing. With this in mind, the increase in halogen size is of particular interest, as larger halogens open up the possibility towards a more dynamic crystal packing, with the size of the atom influencing the packing pattern achieved. Five crystals structures (**24**, **25**, **27**, **30B**, and **32**) have been determined in this series with fluorine being the smallest and bromine being the largest halogen atoms included.

The structure of **24** shows several interactions between the hydrogen and fluorine atoms (Figure 4). The first of these is the reciprocated C–F···H contact between the F1···H17E (2.447(1) Å, 102.7(1)°) (Figure 4a). This tethers the *para*-fluoro atom to the ethyl group of the porphyrin ring. The second contact F2···H202 (2.447(1) Å, 102.7(1)°) binds the *para*-fluoro atom to the aromatic hydrogens on the opposite side of the porphyrin ring (Figure 4b). This has the effect of forming a cupping type pattern between overlapping porphyrin molecules involving three macrocycle rings. In addition, there is a type of edge-on interaction of porphyrin rings, facilitated by a C–F···H contact (2.442(1) Å, 120.4(1)°) between the F3···H106, forming a tight network between the macrocycle planes (Figure 4c).

These interactions can also be highlighted using fingerprint plots (Figure S18a) and Hirshfeld surfaces (Figure S18b). In the Hirshfeld surfaces the H···F contacts can be seen to be centered aryl moiety with the highest contribution (denoted by the heavy red spots) between the fluorine atoms and the *ortho*-hydrogen atoms. There is a secondary but far weaker interaction between the ethyl groups and the fluorine atoms indicated by a pale blue color. Comparing this to the fingerprint plots it can be seen that 19.5% of all surface contacts are involved F···H interactions compounding the low overall contribution to while still remaining directive in the crystal

packing. As a result, a tight packing pattern with the overlapped cupping and the edge-on interactions contributing towards the presence of a little space between the porphyrin layers as seen in Figure S19.
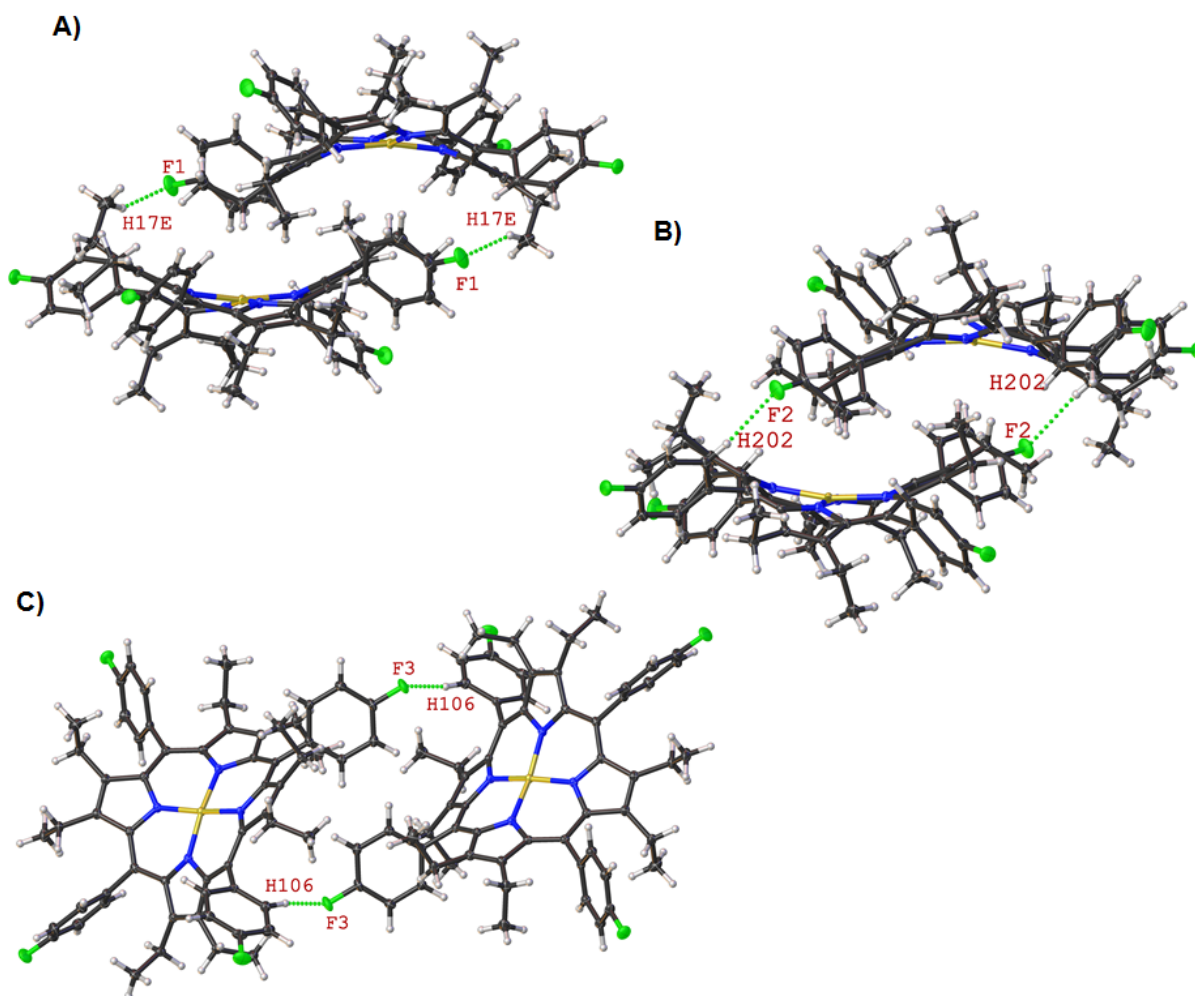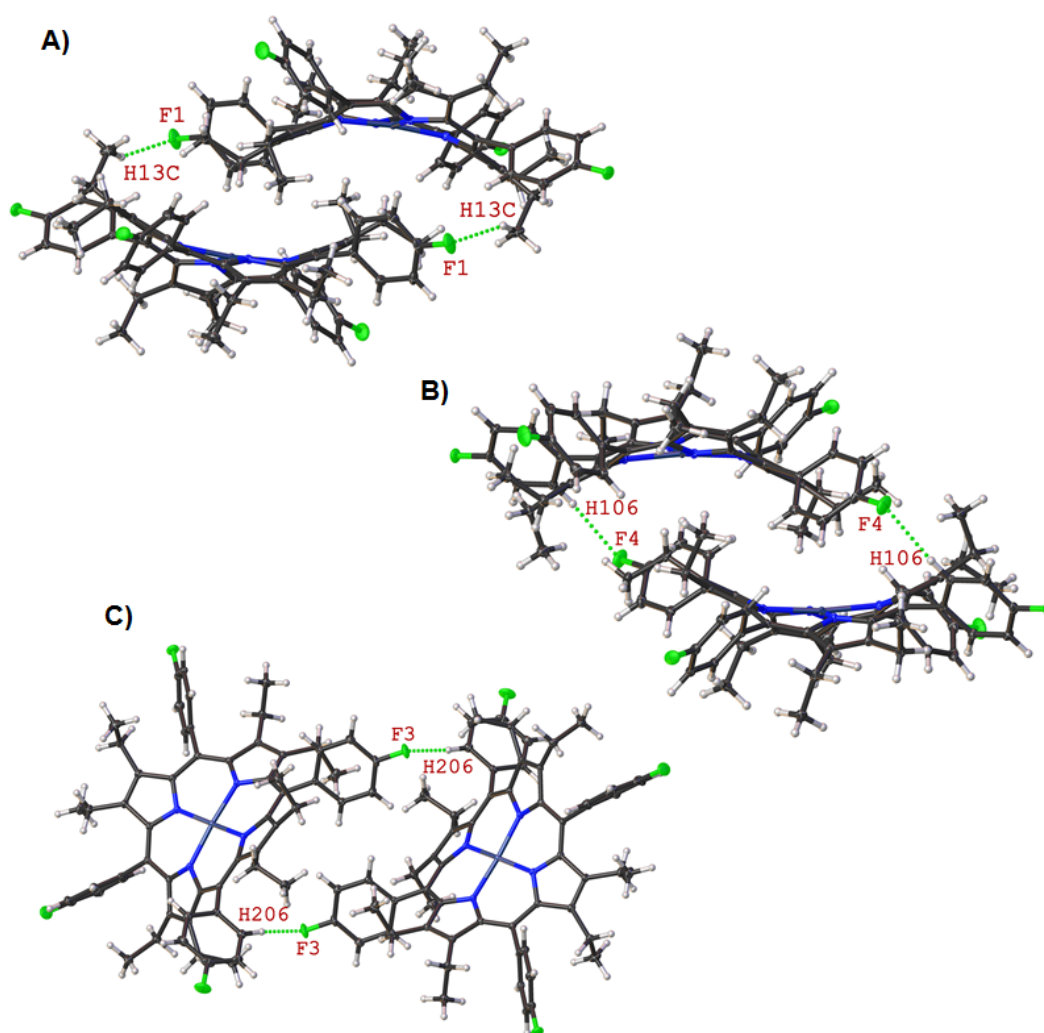

Figure 4: Expanded view of compound **24** showing the H···F contacts involved in the face-to-face (A and B, C–F1···H17E (2.447(1) Å, 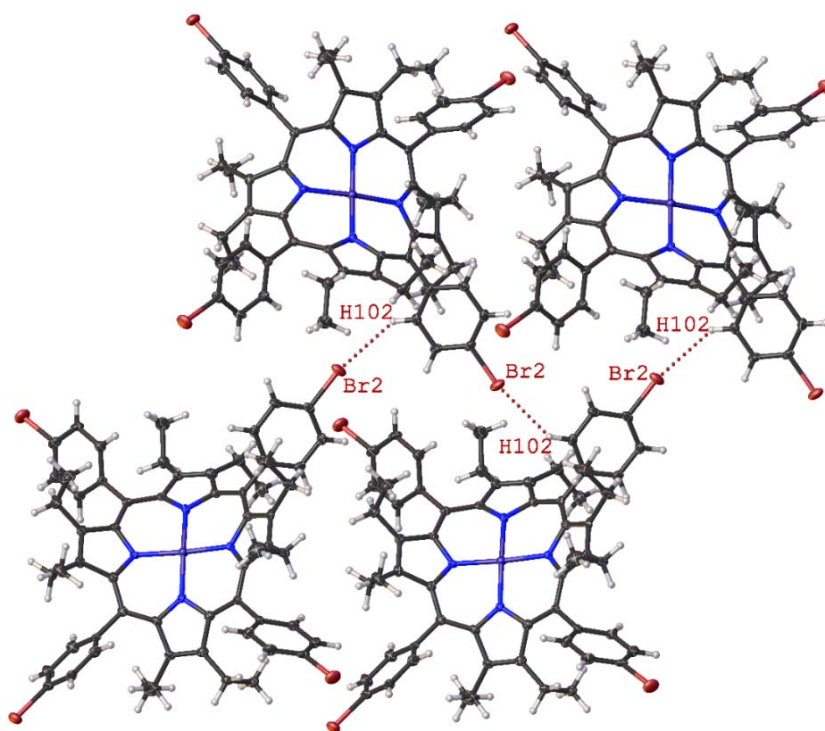102.7(1)°) and C–F2···H202 (2.447(1) Å, 102.7(1)°)) and edge-on interactions (C, C–F3···H106 (2.442(1) Å, 120.4(1)°)). Thermal displacement is given at 50% probability. Interactions are indicated by green dashed lines.

The structure of **25** shows similar types of interactions as seen in **24**, in which the C–H···F interaction is between F1···H13C (2.502(2) Å, 107.5(1)°) and F4···H160 (2.507(2) Å, 136.1(1)°). This, as before, binds three of the macrocycles in the aforementioned cupping pattern (Figure 5). The edge-on interaction is seen between F3···H206 (2.435(2) Å, 118.6(1)°) and results in a similar tight network between the macrocycle planes as with compound **24** (Figure 4). This is validated by comparing the fingerprint plot (Figure S20A) and Hirshfeld surfaces (Figure S20B) which are identical to that of compound **24** with most of the H···F interactions centered on the aryl moiety, specifically the *ortho*-hydrogen atoms. While looking down the *a*-axis of the crystal packing (Figure S21) the offset overlapped pattern caused by the cupping interaction between the porphyrin is quite evident and the edge-on interactions hold the porphyrin macrocycle in almost rhombic shape.

The structure of **27** marks the first increase in the size of the halogen. This results in quite a dramatic change in the nature of halogen-hydrogen interactions. There are no interactions involved in the overlapped cupping pattern seen in the fluorine counterparts and the reciprocal nature of the interactions has now been eliminated. This is seen through the two Cl···H interactions between the Cl2_2···H17E_1 (2.864(7) Å, 97.9(8)°) and Cl2_1···H17D_2 ((2.854(7) Å, 133.3(8)°). This forms a linear network of Cl···H contacts between the two independent molecules which are repeated throughout the structure (Figure 6). The Hirshfeld surface analysis (Figure S22b) show that most of the Cl···H interactions between the porphyrin macrocycles are directed towards the ethyl groups and the edge of the porphyrin. This is different from the fluorine derivatives above where the F···H interactions favored the aryl moiety. The fingerprint plot (Figure S22A) shows that there is a greater surface area covered by the Cl···H interactions (23.3%), however, both the Hirshfeld surface analysis and the general blue color of

the fingerprint plot indicated that these interactions are rather weak compared to the 4-fluoro compounds above. The minor change observed here appear to have a profound change in the crystal packing of compound **27**. As seen in Figure S23, the cupping pattern observed previously in the fluorine series is now combined with face-to-face layered type pattern. The first two rows of porphyrins form a channel with the next layer partaking in cupping pattern (Figure S23). This pattern is repeated through the crystal packing in a 2×2 network looking down the *b*-axis.

Figure 5: Expanded view of compound **25** showing the H⋯F contacts involved in the face-to-face (A and B, C–F1⋯H13C (2.502(2) Å, 107.5(1)°) and C–F4⋯H160 (2.507(2) Å, 136.1(1)°))

and edge-on interactions (C, C–F3$\cdots$H206 (2.435(2) Å, 118.6(1)°)). Thermal displacement is given at 50% probability. Interactions are indicated by green dashed lines.
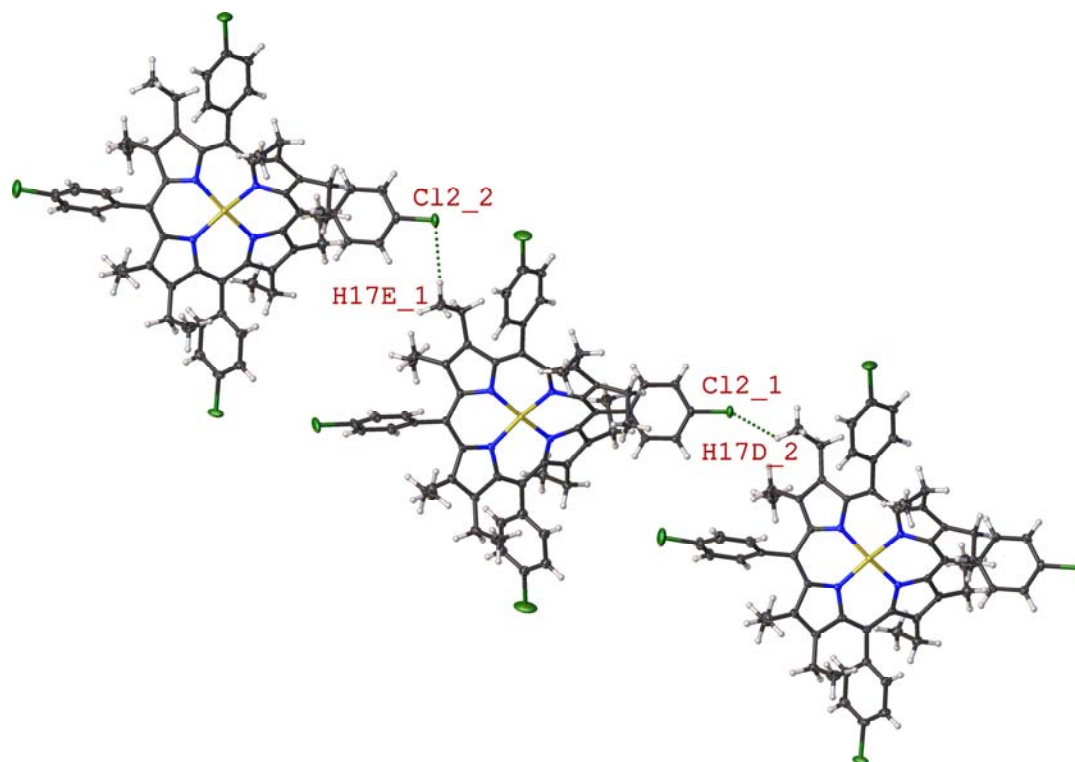
Figure 6: Expanded view of compound **27** showing the H$\cdots$Cl contacts involved in the edge-on interactions C–Cl2_2$\cdots$H17E_1 (2.864(7) Å, 97.9(8)°) and C–Cl2_1$\cdots$H17D_2 ((2.854(7) Å, 133.3(8)°). Thermal displacement is given at 50% probability. Interactions are indicated by green dashed lines.

The inclusion of a bromine atom marks the final increase in halogen size. There are two structures involved in this section, compound **32** and **30B**. For the Cu(II) derivative, compound **32**, the first interaction is between C–Br2$\cdots$H102 (3.026(5) Å, 159.9(1)°) (Figure 7) and results in a Br$\cdots$H network between the *para*-bromine of one porphyrin macrocycle and the *ortho*-hydrogen of the next porphyrin ring in a head-to-head pattern. This is coupled with a second

Br⋯H contact between C–Br2⋯H155 (3.051(6) Å, 98.2(1)°) which forms an orthogonal orientation between the porphyrin macrocycles, partnered with a face-to-face interaction between the two hydrogen contributing porphyrin rings (Figure 8). The final short contact of note is that between C–Br2⋯Br3 (3.867(8) Å, 106.4(1)°) which is reciprocated between porphyrin rings and aids in forming linear sheets of repeating porphyrin head-to-head dimers (Figure 8).

Figure 7: Expanded view of compound **32** showing H⋯Br intermolecular contacts (C–Br2⋯H102 (3.026(5) Å, 159.9(1)°)) involved in the edge-on interactions. Thermal displacement is given at 50% probability. Interactions are indicated by red dashed lines.

The fingerprint plots (Figure S24a) show that the H⋯Br interactions occupy 22.8% of the total surface contacts with a large count of surface points indicated by the blue to light blue color over a narrow spread. When translated to the Hirshfeld surfaces (Figure S24b), it can be seen that most of the Br⋯H interactions are centered on the aryl groups with little indication of any ethyl

group contribution to such interactions. The Br⋯H interactions resemble the fluorine series in character more than that of the chlorine series above. The crystal packing of compound **32** resembles that of compound **27**, where the face-to-face channels of porphyrins coupled with the next layer forming the cupping pattern, appears to be inherent for this class of compound, Figure S25. What is of high interest is the arrangement of the Br⋯H and Br⋯Br interactions as they are placed throughout the crystal system as a whole. From Figure S25, it is clear that Br⋯Br interactions are strictly between the channel section of the packing arrangement. Also, the Br⋯H interactions are the driving force behind that of the cupping pattern is seen in this series forming quite an elaborate mesh-like network throughout the crystal packing.
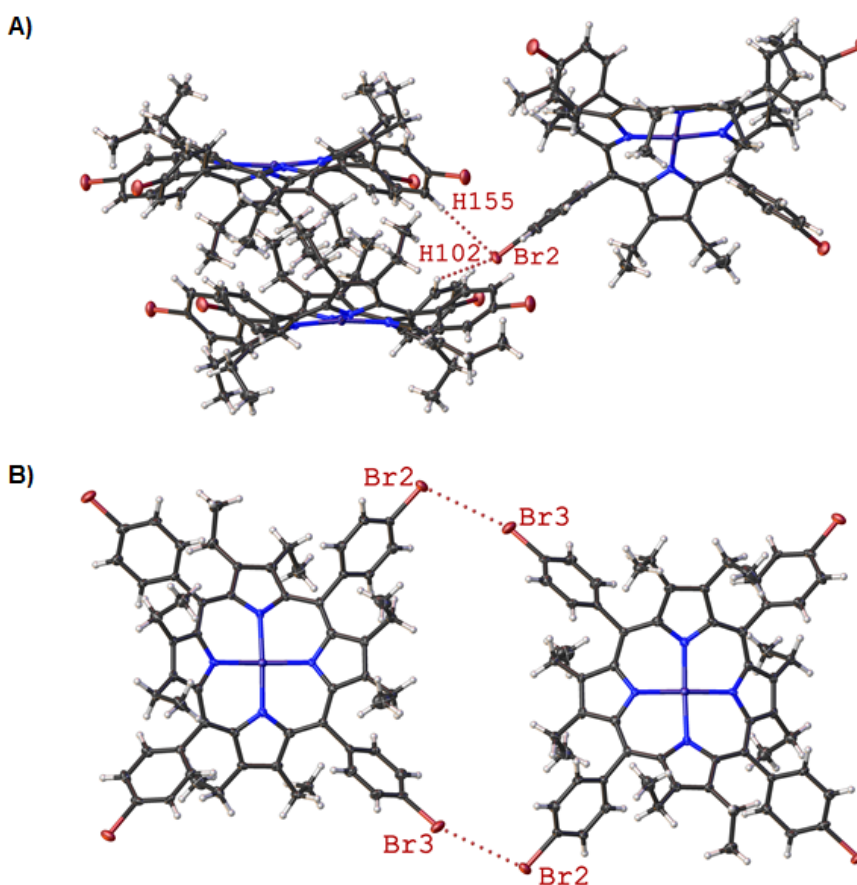
Figure 8: Expanded view of compound **32** showing H···Br (A, C–Br2···H102 (3.026(5) Å, 159.9(1)°) and C–Br2···H155 (3.051(6) Å, 98.2(1)°)) and Br···Br (B, C–Br2···Br3 (3.867(8) Å, 106.4(1)°)) intermolecular contacts involved in the edge-on interactions. Thermal displacement is given at 50% probability. Interactions are indicated by red dashed lines.

The final compound in this section is **30B**. The structure of **30B** is unique to this increasing halogen size series as it is the only solvent containing 4-halo substituted OETArXP. The halogen contact, C–Br3···Br4 (3.738(5) Å, 102.2(9)°), is similar to the short contact seen in compound **32** and gives rise to edge-on interactions between the porphyrin rings (Figure 9). On the opposite side of the macrocycle, there are two Br···H contacts, C–Br1···H106 (2.990(4) Å, 160.8(1)°) and C–Br2···H31A (2.979(4) Å, 129.5(9)°) (Figure 9). This binds four porphyrin macrocycles through halogen-halogen and halogen-hydrogen interactions which are repeated and expressed throughout the unit cell. This is shown quite clearly in the Hirshfeld surfaces analysis for compound **30B**, where all Br···H contacts can be seen to interact with the ethyl and aryl moieties as indicated by the blue shading (Figure S26b). Looking at the fingerprint plots it is noted that H···Br interactions occupy 22.9% of the total surface contacts with a blue to light blue shading indicating a large count of surface points. The packing for compound **30B** is where the true difference lies, however. The basic structure is much the same as that of compound **32**, with the formation of the channel type pattern, driven by the same of Br···H and Br···Br interactions (Figure S27). However, there is a clear difference when looking at the cupping motif. It has been essentially eliminated due to the presence of the CH_2Cl_2 solvent molecules throughout the structure and has created a second perpendicular channel which is occupied exclusively by solvent molecules, whereas the original channel motif is completely solvent free. This change in crystal packing is a direct result of the inclusion of the solvent.
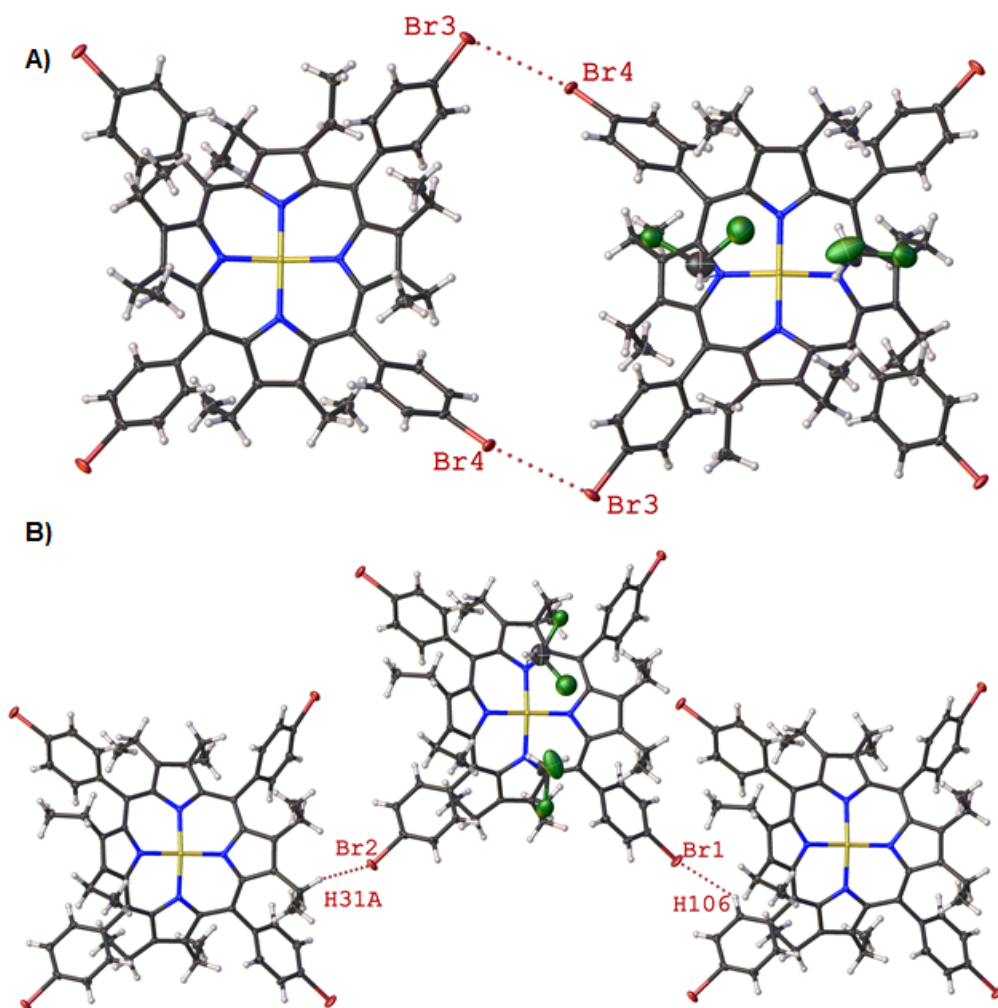
Figure 9: Expanded view of compound **30B** showing the Br···Br (A, C–Br3···Br4 (3.738(5) Å, 102.2(9)°)) and H···Br (B, C–Br1···H106 (2.990(4) Å, 160.8(1)°) and C–Br2···H31A (2.979(4) Å, 129.5(9)°)) intermolecular contacts involved in the edge-on interactions. Thermal displacement is given at 50% probability. Interactions are indicated by red dashed lines.
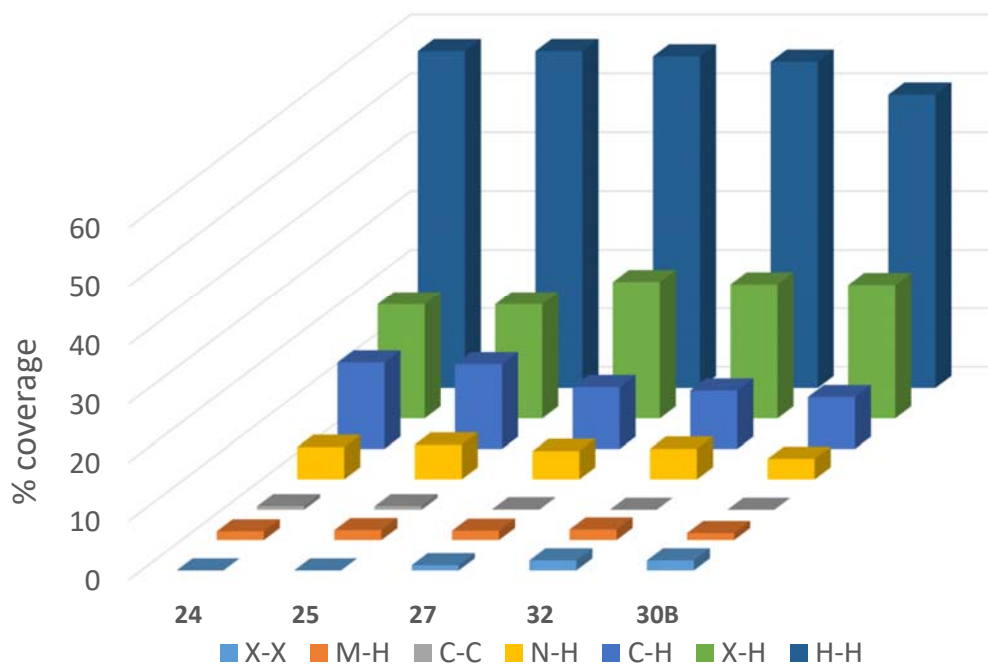
Figure 10: Relative contributions of the various noncovalent contacts to the Hirshfeld surface area in complexes **24**, **25**, **27**, **32**, and **30B**.

From this section, it can be seen that the main difference between these compounds is due to the preferred intermolecular interactions each porphyrin demonstrates. This is indicated by the fluorine series having an equal preference for alkyl or aryl groups (*ortho*-hydrogen), the chlorine series favoring interactions between the alkyl groups, and the bromine appearing to favor the aryl (*ortho*- and *meta*-hydrogens). Although the sample size is currently limited, this halogen-hydrogen interaction preference is directed by each specific halogen. The other difference is that both fluorine and chlorine do not initiate halogen-halogen interactions, with only the bromine series showing this so far. Looking at the relative contributions of the various noncovalent contacts to the Hirshfeld surface (Figure 10) this can be clearly seen through the X⋯X and the X⋯H contacts where there is a subtle increase in both these fields going from fluorine to

bromine coupled with a decrease in the C···H and H···H fields. Finally, while the effects of different metal(II) centers appear to have no influence on the packing, while the inclusion on the solvent has quite a stark change on the crystal packing.

Changing the Position of the Halogen. In this section, the effects of altering the substitution pattern of a halogen from 4-position to the 2,6-position will be investigated. Six new 2,6-dihalo-substituted structures were obtained (**18A**, **36**, **38A**, **39**, **40**, and **40A**). In general terms, this has some significant effects on the type of interactions that are now available to the porphyrin macrocycle, namely the presence of intramolecular interactions. The effects will be discussed in comparison to their 4-substituted derivates.

The first structure is that of compound **36** where the aryl ring of the porphyrin contains a di-*ortho*-fluoro substitution. In this structure, two independent molecules are present in the asymmetric unit. From Figure S28 the inclusion of intramolecular H···F bonds is quite evident. In fact, this is the most common type of interaction seen in this structure. In both residue one and two, the fluorine atoms show a high preference for interacting with the CH_2 hydrogen atoms of the ethyl chain. This is exemplified in the Hirshfeld surface analysis (Figure S29) where the density of F···H interactions surrounding the ethyl and aryl groups is higher than that in compound **24**. However, this interaction has little effect on the actual packing of the molecule. Instead, there are several other H···F short contacts present in the structure that result in three distinct intermolecular interactions, forming the overall packing arrangement (Figure 11). The first two are the edge-to-face interactions between the two residues aided by H···F contacts between F4_2···H13E_1, F5_2···H12D_1, and F3_1···H17E_2. The second type is an edge-on interaction between the aryl rings aided by F5_1···H53_1 and F1_1···H53_1. The combination of these two types of interactions results in a densely packed crystal structure with individual

porphyrin molecules held at right angles to each other through H···F contacts (Figure S30). This type of packing is quite different from that of compound **24** as the overlapped cupping pattern has been replaced by an edge-to-face packing arrangement.
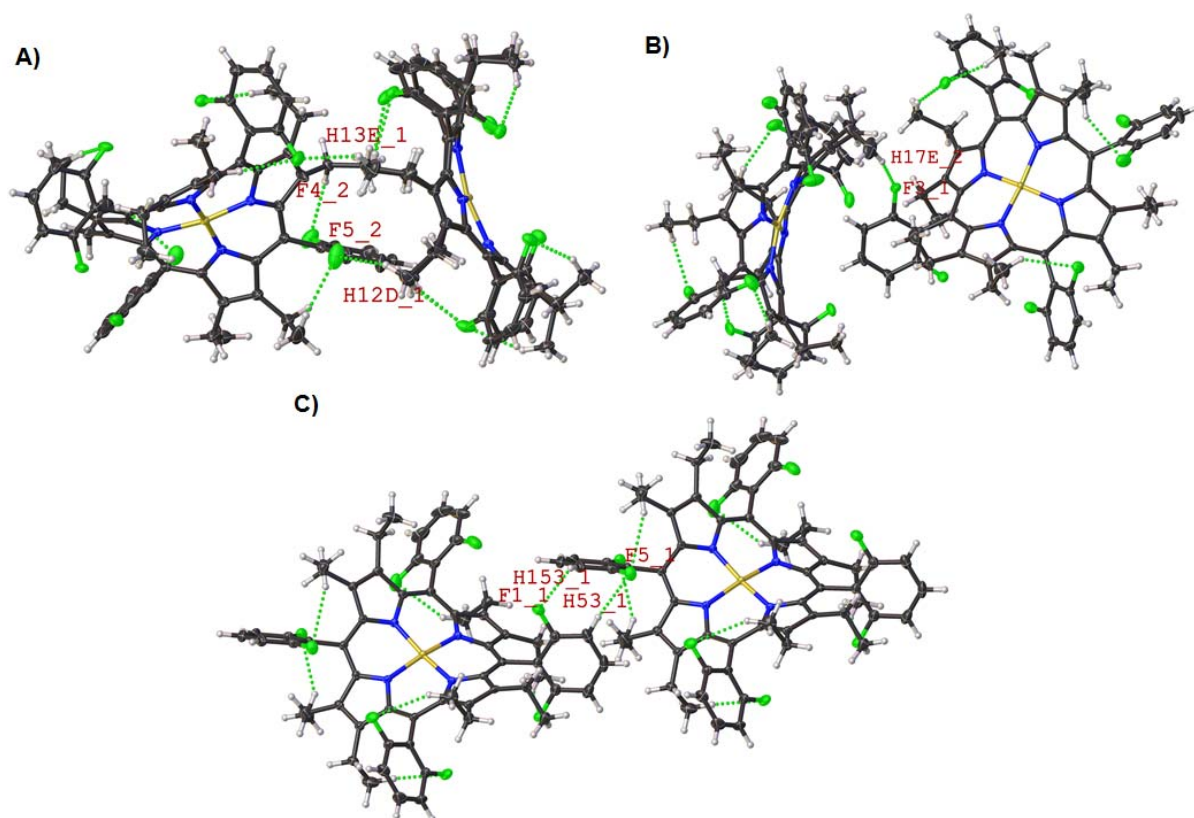

Figure 11: Expanded view of the three intermolecular interactions of compound **36** showing the H···F intermolecular (A, C–F4_2···H13E_1 (2.405(2) Å, 118.0(1)°) and C–F5_2···H12D_1 (2.645(2) Å, 117.3(1)°)) (B, C–F3_1···H17E_2 (3.377(2) Å, 137.7(1)°)) contact involved in the face-to-face or edge-on (C, C–F5_1···H53_1 (2.730(1) Å, 104.2(1)°) and C–F1_1···H53_1 (2.602(2) Å, 100.7(1)°)) interactions. Thermal displacement is given at 50% probability. Interactions indicated by green dashed lines. Each image is a separate view of the crystal structure to allow for the simple presentation of each interaction independently.

The next five structures (**18A**, **38A**, **39**, **40**, and **40A**) all belong to the series of 2,6-dichlorophenyl substituted porphyrin complexes with a variety of free base, metal(II) centers, and solvent (CDCl$_3$) included. This is the largest family of structures in this work and offers the best dataset to investigate subtle differences within the OETArXP series. There are some general features that all these structures share. This is the propensity to partake in intramolecular interactions between the chlorine atoms and the terminal hydrogen atoms of the ethyl chains. This feature is typical of the 2,6-halo series, as both the chlorine and fluorine derivatives share this motif. The pattern in which these intramolecular interactions take place is not identical from structure to structure, such as, 2,6-dichlorophenyl substituted at the 15-position of **18A** does not partake in this intramolecular interaction. These differences can be due to several factors such as the intermolecular contacts involved or solvent inclusion/exclusion. However, it should be noted that these intramolecular interactions play no role in packing or any particular binding motif, and therefore should not be considered an important structural factor. Figure S31-S32 includes the Hirshfeld surface analysis and fingerprint plots of the 2,6-dichlorophenyl substituted porphyrin. Looking at these plots we can see only minor changes due to the inclusion of solvent which results in a higher density of Cl···H interactions in the core of the porphyrin. Other noticeable features are the Cl···H contacts which are mostly due to the intramolecular interactions and as such obscure any possible analysis of the intermolecular interactions using this method.

The structure of **18A** contains one intermolecular interaction C–Cl7···H154 (2.935(3) Å, 78.5(4)°) which creates an edge-on contact between the porphyrin macrocycle similar to that of compound **27** (Figure 12). However, whereas the Cl of compound **27** interacts with the ethyl groups, in **18A** they interact with the aryl groups exclusively. As this structure is both free base and solvated with CDCl$_3$, the structure is separated into layers of porphyrin with a solvent

channel between them. This alters the packing pattern slightly compared to the *para*-chloro-substituted porphyrin **27**, resulting in a wider packing pattern (Figure S33). This is due to both the solvent inclusion and the alternate intermolecular interaction as stated above.
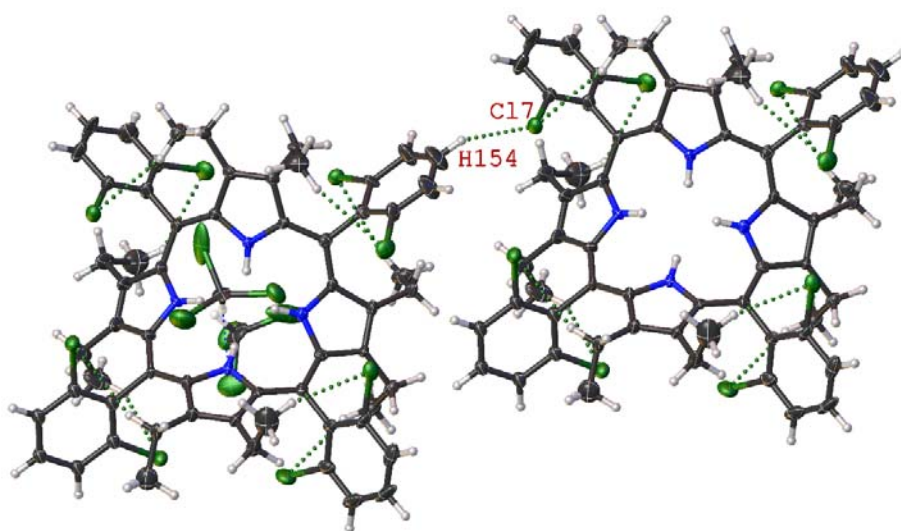
Figure 12: Expanded view of compound **18A** showing the Cl⋯H intermolecular contact (C–Cl7⋯H154 (2.935(3) Å, 78.5(4)°)). Thermal displacement is given at 50% probability. Interactions indicated by green dashed lines.

The structure of **38A** is the Ni(II) version of **18A**. In Figure 13, it is shown that compound **38A** appears to favor a face-to-face interaction between the porphyrin macrocycles through Cl8⋯H82A, as opposed to the edge-on interaction favored by compound **18A**. In the packing diagram, even though the primary intermolecular interactions are quite different the overall crystal packing is almost identical (Figure S34). This suggests two things are occurring in the crystal packing. The first and most obvious is that the solvent has more of an impact on the packing of the structure than the inclusion of a metal to the core of the porphyrin. The second

and more subtle is that the metal(II) center has a minor effect by changing the intermolecular interaction from an edge-on interaction towards a face-to-face interaction.
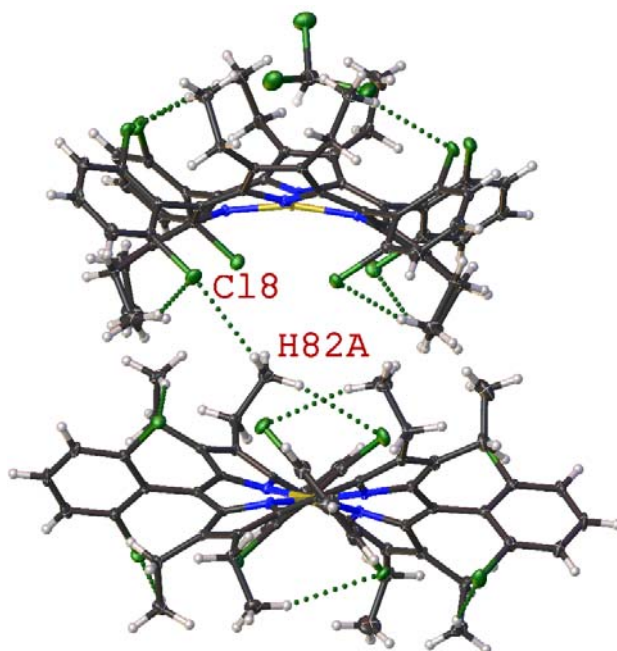
Figure 13: Expanded view of compound **38A** showing the Cl···H intermolecular contact involved in the face-to-face interactions (C–Cl8···H82A (2.876(1) Å, 169.4(1)°)). Thermal displacement is given at 50% probability. Interactions indicated by green dashed lines.

The structure of **39** is that of the Pd(II) derivative of the 2,6-dichlorophenyl series. This is the first of two non-solvated structures in this series. Where the main difference arises is with the intermolecular interactions. In this structure, a new type of contact is observed in which the edge of one porphyrin macrocycle interacts with the face of its nearest neighboring porphyrin macrocycle (Figure 14). This is aided by two Cl···H interactions (Cl2···H82A and Cl4···H32A) and is reproduced on the opposite side of the porphyrin ring, due to symmetry. This results in forming a network, where one porphyrin macrocycle is essentially sandwiched between the face

of two other porphyrin rings. This is also the position which was previously occupied by CDCl₃ making this interaction profile unique to the non-solvated structures in this series. The effect these interactions have on the packing is quite stark. Rather than the alternating layers of porphyrins and solvent previously seen in this series, there is now a highly ordered stacked system, in which the phenyl rings are stacked on top with each other (Figure S35), as opposed to the solvent driven packing as seen before in compound **38A**.
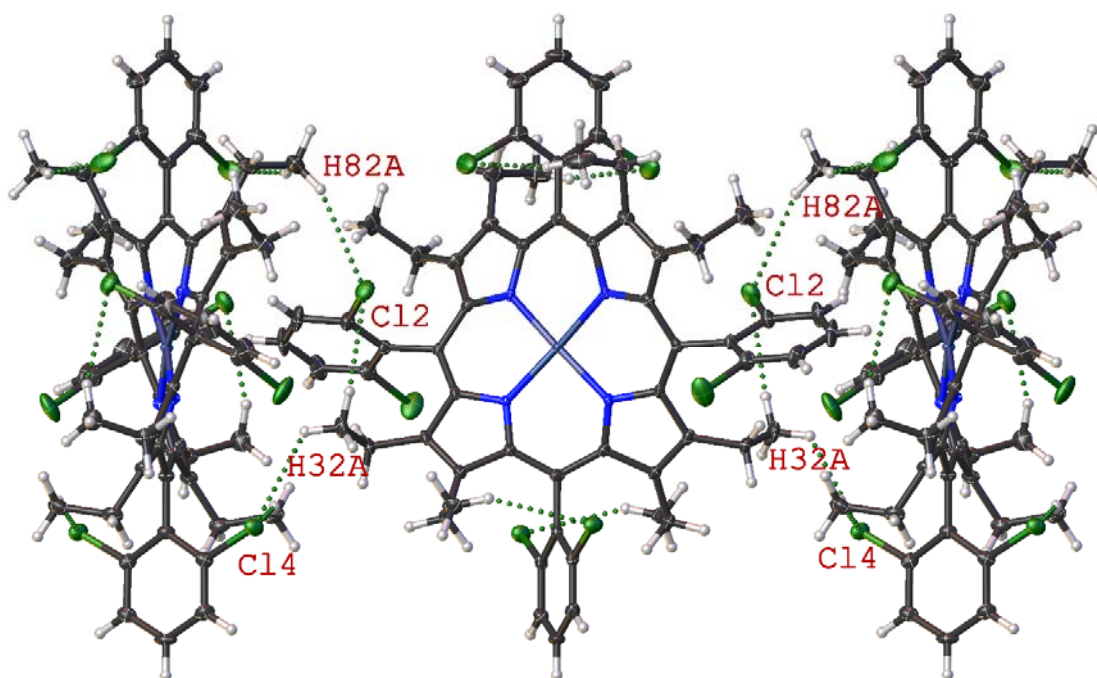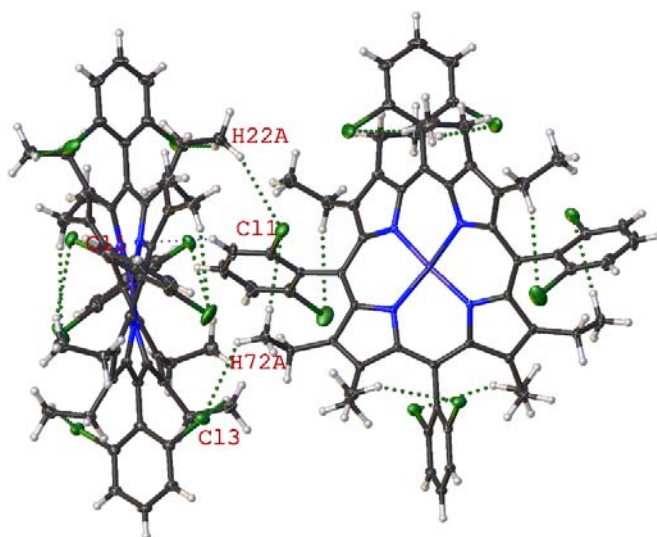

Figure 14: Expanded view of compound **39** showing the Cl···H intermolecular contacts involved in the face-to-edge interactions (C–Cl2···H82A (2.907(8) Å, 109.8(1)°) and C–Cl4···H32A (2.851(8) Å, 141.8(1)°). Thermal displacement is given at 50% probability. Interactions indicated by green dashed lines.

The structure of compound **40** is the Cu(II) derivative of the 2,6-dichlorophenyl series. This is the second of the two non-solvated structures in this series. This structure is almost identical to
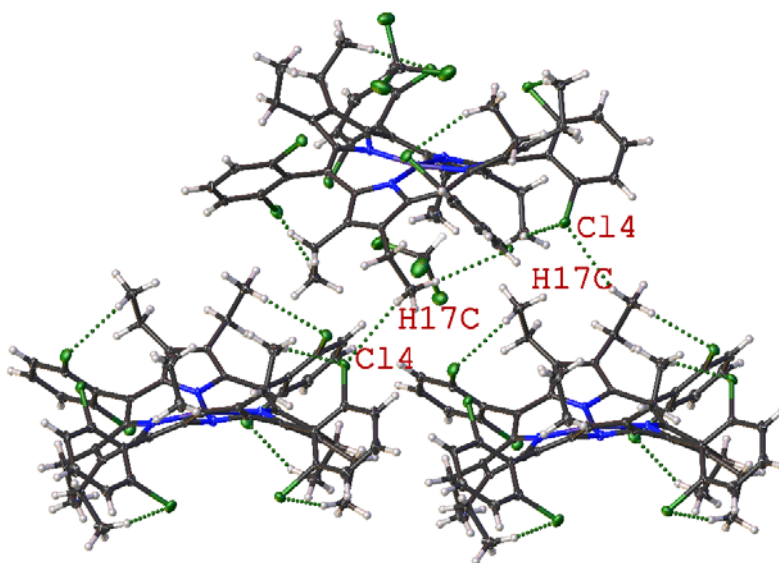
that of compound **39**. The intermolecular interactions are the exact same as seen in compound **39**, where the one porphyrin ring is held between the faces of two other porphyrin macrocycle in a face-to-edge packing pattern. The interactions involved in this motif are C–Cl1⋯H22A (2.900(6) Å, 103.6(8)°) and C–Cl3⋯H72A (2.882(6) Å, 143.9(2)°) and are reproduced on the opposite side of the porphyrin ring due to symmetry, Figure 15. When looking at the packing of compound **40**, it is clear that there are little to no differences between it and that of compound **39**, (Figure S36). This is a clear indication that the metal(II) centers chosen in this project, have little to no effect on the overall structure and packing of these compounds in this 2,6-di-substituted series.


Figure 15: Expanded view of compound **40** showing the Cl⋯H intermolecular contacts involved in the face-to-edge interactions (C–Cl1⋯H22A (2.900(6) Å, 103.6(8)°) and C–Cl3⋯H72A (2.882(6) Å, 143.9(2)°)). Thermal displacement is given at 50% probability. Interactions indicated by green dashed lines.

The structure of compound **40A** is the CDCl$_3$ solvated structure of porphyrin **40** and as such, is the first case in which only the solvent effects can be examined without any other external factors. The intermolecular interactions of compound **40A** in this structure are different from those of **40**. Rather than the face-to-edge interactions previously seen in **40**, compound **40A** shows an offset face-to-face network, which is aided by a Cl⋯H network (C–Cl4⋯H17C (2.943(1) Å, 125.9(2)°)). This is repeated throughout the structure in a wave-like pattern, tethering lines of porphyrin together, Figure 16. However, the crystal packing is identical to that of **38A** and **18A** which indicates the solvent inclusion is more directive in the crystal packing than the intramolecular/intermolecular interactions, Figure S37.

Figure 16: Expanded view of compound **40A** showing the Cl⋯H intermolecular contact involved in the face-to-face interactions (C–Cl4⋯H17C (2.943(1) Å, 125.9(2)°)). Thermal displacement is given at 50% probability. Interactions indicated by green dashed lines.
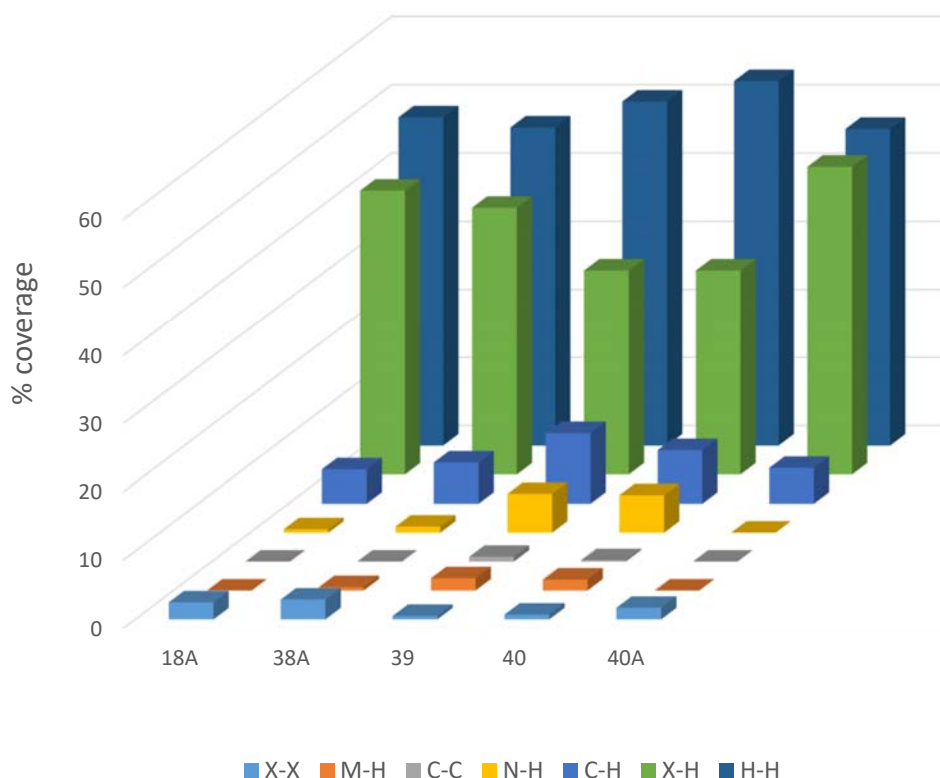
Figure 17: Relative contributions of the various noncovalent contacts to the Hirshfeld surface area in complexes **18A**, **38A**, **39**, **40**, and **40A**.

Overall, this section highlights some key features. The first of these is that the metal(II) centers have very little effects on the overall crystal packing. This is indicated by the fact that, even if structures contain Cu(II), Ni(II), or free base, a similar packing motif is observed. The only difference observed is when the structure contains a solvent molecule. This leads to the second observation. The inclusion or exclusion of solvent is the main driving force in packing. When the compounds exclude any solvent molecules, a face-to-edge interaction is observed. However, the face-to-face overlap is exclusively observed in the solvated structures. When examining the relative contributions of the various noncovalent contacts to the Hirshfeld surface area (Figure

17), it can be noted that in solvated structures (**18A**, **38A**, and **40A**), the contribution to the H···H, X···H, and N···H are all increased and the contribution to the N···H, M···H, and C···H contacts are all decreased relative to the non-solvated structures (**39** and **40**).

Nitrile porphyrins: For the nitrile porphyrins, compound **41** is atypical of a rigid hydrogen-bond acceptor. This is exemplified in Figure 18, where the cyano group is seen to be directive towards *ortho*-aryl hydrogen atoms in a bifurcated fashion. This is directed through C–N1···H52 (2.720(1) Å, (130.5(1)°) and C–N1···H206 (2.730(1) Å, 95.8(1)°), in which the two interacting porphyrin molecules are orthogonal to each other. The second interaction profile is seen between C–N2···H53 (2.675(2) Å, 131.6(1)°) (Figure 19). This results in an interesting feature in which these two porphyrin macrocycles are held at an angle of 59.1(3)° as measured by their 24-atom least-squares plane. This motif is repeated throughout the structure and results in a Z-shaped pattern through the layer of porphyrin rings (Figure 20). These two interaction profiles combine to make the packing of this porphyrin exclusively on the periphery. Looking at the Hirshfeld surface analysis it is clear that all N···H interactions happen on the edge of the porphyrin macrocycle and strictly involve the aryl hydrogen atoms as indicated by the blue shading (Figure S38b). When comparing to the fingerprint plot (Figure S38a) it is apparent that with 21.5% of the total surface contacts resulting from the N···H of the periphery CN moiety and as can be seen with the blue-green shading demonstrating the high surface points are associated with the N···H$_{aryl}$ interactions. This highly ordered N···H contact arrangement results in the tightly ordered packing seen in Figure S39.
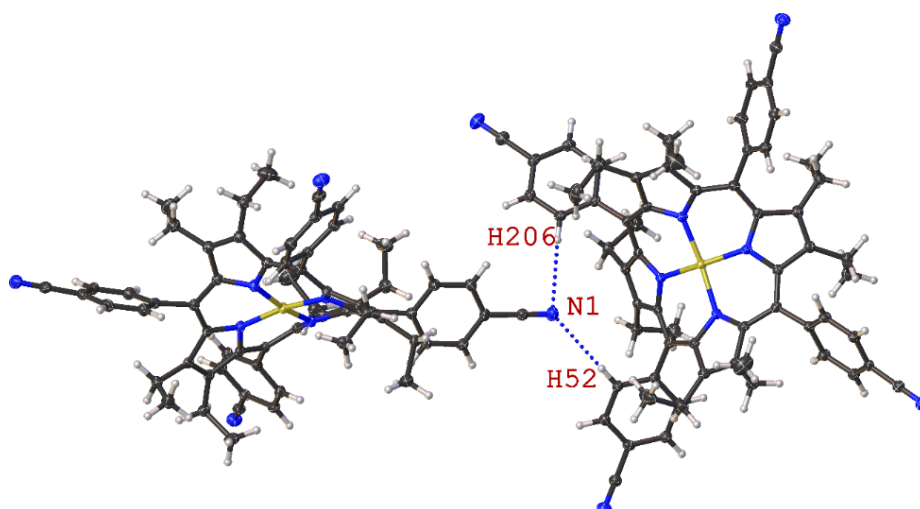
Figure 18: Expanded view of compound **41** showing the N···H intermolecular contacts involved in the bifurcated interactions (C–N1···H52 (2.720(1) Å, (130.5(1)°) and C–N1···H206 (2.730(1) Å, 95.8(1)°)). Thermal displacement is given at 50% probability. Interactions are indicated by blue dashed lines.
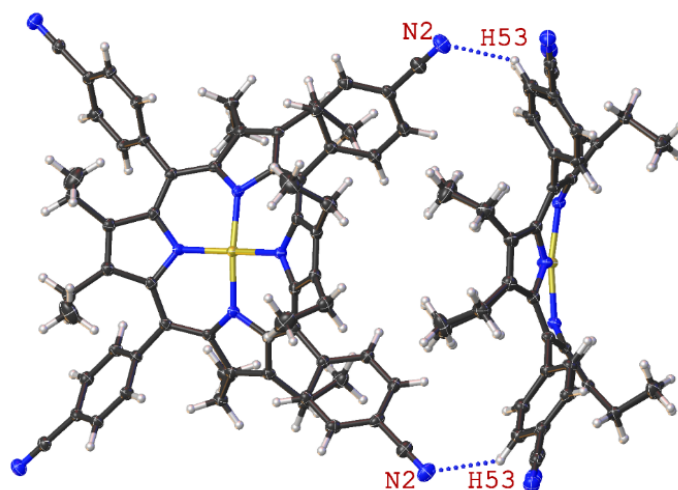
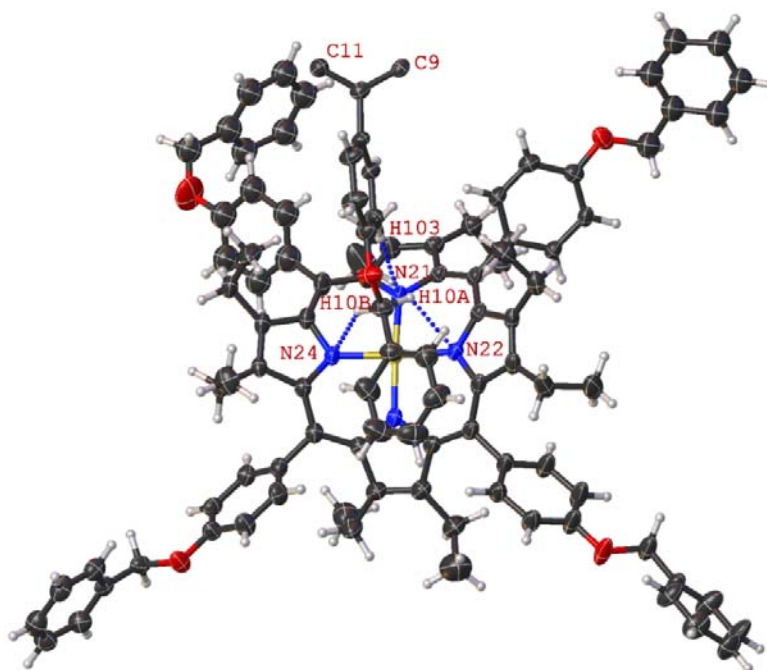**Figure 19:** Expanded view of compound **41** showing the N···H intermolecular contacts involved in the edge-on interactions (C–N2···H53 (2.675(2) Å, 131.6(1)°)). Thermal displacement is given at 50% probability. Interactions are indicated by blue dashed lines.
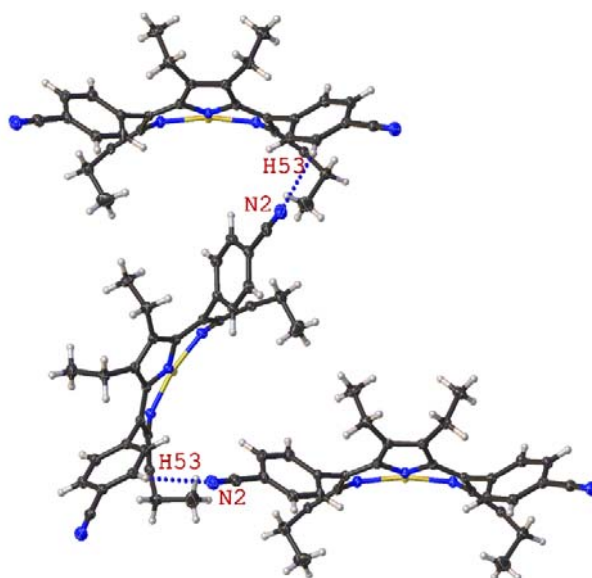
Figure 20: Expanded view of compound **41** showing the N2···H53 intermolecular contacts (C–N2···H53 (2.675(2) Å, 131.6(1)°)) involved in the Z-shaped pattern through the layer of porphyrin rings. Thermal displacement is given at 50% probability. Interactions are indicated by blue dashed lines.

'Chain' porphyrins. In the structure of **45**, two independent molecules were isolated in the asymmetric unit and all atoms have been assigned a residue number in the form of '_#'. For this structure, the core interactions have two types of motifs. The first of these is where the *meta*-hydrogen atom of the phenyl ring is involved in a short contact with the N21 (C103_2–H103_2···N21_1) at a distance of 2.891(4) Å (Figure 21). The second interaction motif is between the CH_2 hydrogen atoms of the benzyloxy chain and the nitrogen atoms N22 and N24 (C108_2–H10A_2···N22_1 (2.832(3) Å) and C108_2–H10B_2···N24_1 (3.001(4) Å)) (Figure 21). This interaction is interesting due to the fact that the angle caused by the inclusion of oxygen into the benzyloxy chain holds the CH_2 moiety at the same distance away from the porphyrin core as the aromatic CH which is also involved in this core interaction (Figure 22). When a

Hirshfeld surface analysis is applied to this porphyrin structure, it can be seen that the N···H interactions are strictly centered on the aryl and benzyloxy chain as indicated by the blue shading, confirming that these are the only contacts involved with the core of the porphyrin (Figure S40B). However, from the fingerprint plot it can be clearly seen that the contacts are low frequency occupy 3.5% of total surface contacts in a diffuse pattern (Figure S40A). This coupled with the fact that distance of the N···H suggest that these are a nonbonding interaction between the porphyrin molecules. The crystal packing of this structure displays a consistent overlap of the meso-substituent which results in a tightly packed mesh-like crystal pattern (Figure S41).

Figure 21: Expanded view of compound **45** showing the N···H core interactions. Thermal displacement is given at 50% probability. Interactions are indicated by blue dashed lines (C103_2–H103_2···N21_1 (2.891(4) Å, 175.6(3)°), C108_2–H10A_2···N22_1 (2.832(3) Å, 123.1(3)°) and C108_2–H10B_2···N24_1 (3.001(4) Å, 144.6(3)°)). For clarity, the second

porphyrin ring has been cut out of the image at C9 and C11 (these atoms are labeled) to avoid overcrowding.
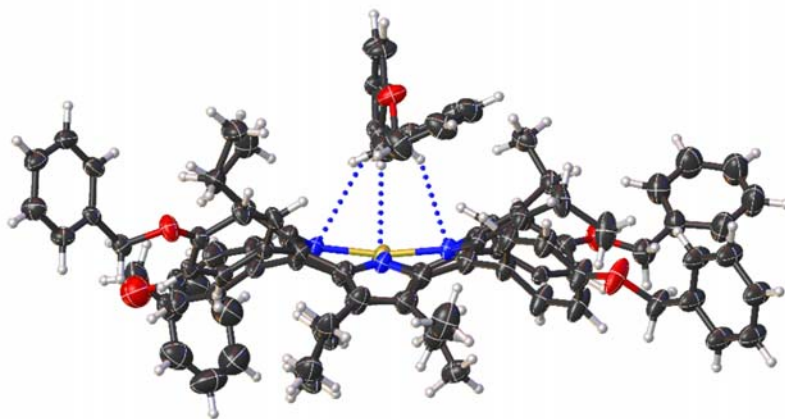
Figure 22: Expanded side view of compound **45** showing the N···H core interactions. Thermal displacement is given at 50% probability. For clarity, the second porphyrin ring has been cut out of the image to avoid overcrowding.

CONCLUSION

In conclusion, the synthesis of several new OETArXP and their metal(II) counterparts was undertaken. The compounds were achieved in moderate to good yields. We also synthesized a novel family of 'arm extended' OETArXPs where X is triazole-linked benzene group with a *para*-functionalized moiety (cyano, nitro, methyl ester, methyl ether, or aldehyde), which introduces an alternate functionality to the OETArXPs by using hydrogen bonding or other functional groups. Not only are the yields sufficiently high, but reaction times are quick and either the azide or acetylene derivatives of OETArXP can be used as a starting point. Additionally, using these systems, a large variety of compounds can be quickly synthesized

through a one-step process, moving away from traditional condensation reactions and the need to synthesize complicated aldehyde precursors.

We have also determined the structures of several new OETArXPs, their metal counterparts, and solvent inclusion complexes. During this work, the aspects of substitution type and pattern, solvent inclusion, and change of metal(II) centers was carried out in order to gauge the effect such alterations might have on the crystal packing.

We have established that increasing the size of the halogen atom affects the potential of intermolecular interactions and the resulting crystal packing in 4-halo-OETArXP complexes (Figure 23). The fluorine series has an equal preference for alkyl or aryl groups (*ortho*-hydrogen), with chlorine favoring interactions between the alkyl groups, and bromine appearing to favor the aryl (*ortho*- and *meta*-hydrogens). Only in 4-bromo-OETArXPs are direct halogen-halogen interactions observed. In the 4-cyano-, 4-benzyloxy-, and the 2,6-halo-OETArXP cases unique conformational arrangements are observed and do not fit the trends seen above e.g. the 4-cyano-OETArXP favors periphery cyano moieties and *meta*-hydrogen atoms; 4-benzyloxy-OETArXP shows unique nonbonding interactions between meso-substituents and the porphyrin core; 2,6-halo-OETArXP features more face-to-face and face-to-edge interactions.
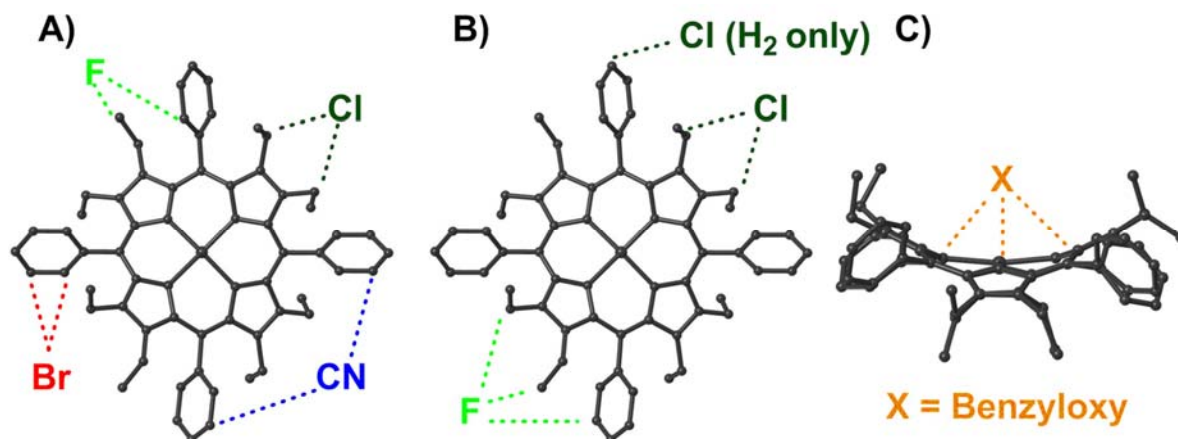
Figure 23: Schematic representation of intermolecular interactions for the 4-substituted-OETArXP (A), 2,6-di-substituted-OETArXP (B), and 4-benzyloxy-OETArXP (C) compounds.

While it was noted that altering the metal(II) centers has only a marginal influence on the local environment of the macrocycle, rather than in the global packing, solvent effects play a much larger role. The inclusion/exclusion of solvent molecules also has a larger impact in the crystal packing than intermolecular/intramolecular interactions and appears to be the major driving force behind crystal packing. This is caused by expanding the distance between the porphyrin layers to accommodate the solvent molecule as demonstrated in Figure 24. It was observed that by including either a DCM or CDCl₃ into the crystal lattice, two alternate forms can be achieved, however, since both structures differ in substituent pattern the question of pattern *vs* solvent remains an area for further investigation on the crystal packing of OETArXP inclusion complexes.
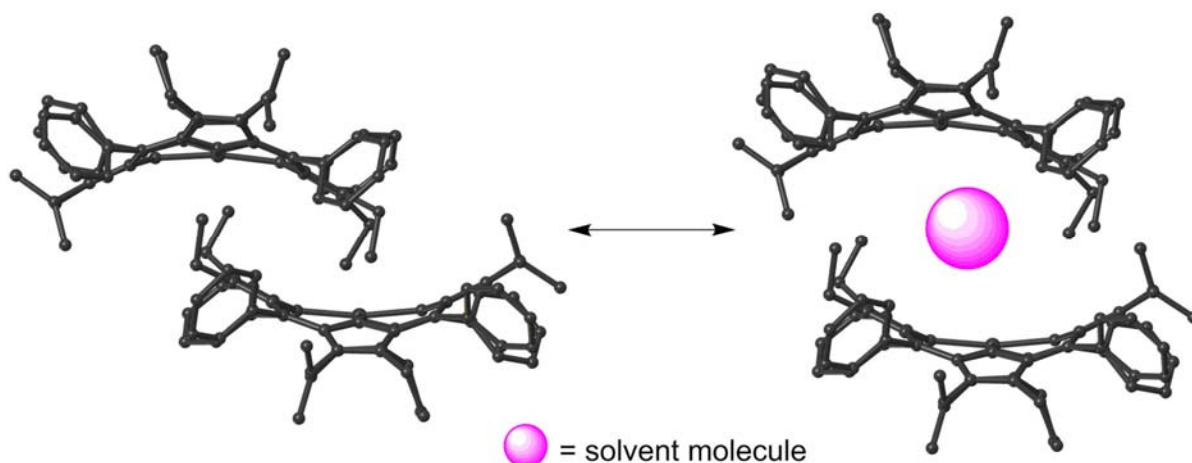
= solvent molecule

Figure 24: Schematic representation of the separation of porphyrin layers due to the inclusion of a solvent molecule.

The crystal packing of this work shows the potential to create selective and functional receptor sites based on free base porphyrins. However, as far as our study indicates, the design of free base nonplanar porphyrin non-covalent organic frameworks through crystal engineering has not yet been realized. The variety of porphyrin packing arrangements herein indicates the need for further studies in this area.

Future work in this area should focus around (a) generating co-crystals with complementary functionalities (such as 4-iodophenyl and 4-cyanophenyl) to direct the intermolecular interactions between the functional groups or to use more hydrogen bonding functionalities as Goldberg and co-workers have previously reported[33] (b) study the solvent inclusion complexes in more detail in an attempt to form clathrates. Investigate how the solvent interacts with the face of the porphyrin through noncovalent interactions by systematically altering these solvent molecules for other small molecules (quinone, anthracenes, aldehydes, etc.). This aspect is similar to the porphyrin sponges reported by Byrn *et al.*, where a variety of guests could be

incorporated into the crystal structure of the OETArXPs to potentially form porphyrin clathrates.[32]

ASSOCIATED CONTENT

Supporting Information. The supporting information is available free of charge on the ACS publications website. The following files are available free of charge.

Supplementary images, experimental details, and characterization, and X-ray crystallography data.

AUTHOR INFORMATION

Corresponding Author

* E-mail: sengem@tcd.ie

Notes

The authors declared no competing financial interest.

REFERENCES

1. Kielmann, M.; Senge, M. O., Molecular Engineering of Free-Base Porphyrins as Ligands-The N-H···X Binding Motif in Tetrapyrroles. *Angew. Chem. Int. Ed.* **2019,** *58*, 418–441.

2. Roucan, M.; Kielmann, M.; Connon, S. J.; Bernhard, S. S. R.; Senge, M. O., Conformational control of nonplanar free base porphyrins: towards bifunctional catalysts of tunable basicity. *Chem. Commun.* **2018,** *54*, 26–29.

3. Senge, M. O.; MacGowan, S. A.; O'Brien, J. M., Conformational control of cofactors in nature – the influence of protein-induced macrocycle distortion on the biological function of tetrapyrroles. *Chem. Commun.* **2015,** *51*, 17031–17063.

4. Senge, M. O., Exercises in molecular gymnastics - bending, stretching and twisting porphyrins. *Chem. Commun.* **2006**, 243–256.

5. Senge, M. O., Highly Substituted Porphyrins. In *The Porphyrin Handbook*, Academic Press: 2000; Vol. 1, pp 239–347.

6. Scheidt, W. R.; Lee, Y. J., Recent advances in the stereochemistry of metallotetrapyrroles. In *Structure and Bonding Metal Complexes with Tetrapyrrole Ligands I*, Buchler, J. W., Ed. Springer Berlin Heidelberg: Berlin, Heidelberg, 1987; pp 1–70.

7. Senge, M. O.; Dahms, K., (5-n-Butyl-10,20-diisobutylporphyrinato)nickel(II). *Acta Cryst. Sect. E* **2014,** *70*, m251.

8. Senge, M. O.; Flanagan, K. J.; Ryan, A. A.; Ryppa, C.; Donath, M.; Twamley, B., Conformational and structural studies of meso monosubstituted metalloporphyrins - Edge-on molecular interactions of porphyrins in crystals. *Tetrahedron* **2016,** *72*, 105–115.

9. Flanagan, K. J.; Mothi, E. M.; Kötzner, L.; Senge, M. O., Crystal structure of [5-n-butyl-10-(2,5-dimethoxyphenyl)-2,3,7,8,13,12,17,18-octaethylporphyrinato]nickel(II). *Acta Cryst. Sect. E* **2015,** *71*, 1397–400.

10. Senge, M. O.; Medforth, C. J.; Forsyth, T. P.; Lee, D. A.; Olmstead, M. M.; Jentzen, W.; Pandey, R. K.; Shelnutt, J. A.; Smith, K. M., Comparative Analysis of the Conformations of Symmetrically and Asymmetrically Deca- and Undecasubstituted Porphyrins Bearing Meso-Alkyl or -Aryl Groups. *Inorg. Chem.* **1997,** *36*, 1149–1163.

11. De Luca, G.; Romeo, A.; Scolaro, L. M.; Ricciardi, G.; Rosa, A., Sitting-Atop Metallo-Porphyrin Complexes: Experimental and Theoretical Investigations on Such Elusive Species. *Inorg. Chem.* **2009,** *48*, 8493–8507.

12. Patra, R.; Chaudhary, A.; Ghosh, S. K.; Rath, S. P., Axial Ligand Orientations in a Distorted Porphyrin Macrocycle: Synthesis, Structure, and Properties of Low-Spin Bis(imidazole)iron(III) and Iron(II) Porphyrinates. *Inorg. Chem.* **2010,** *49*, 2057–2067.

13. Senge, M. O., Axial Ligand Effects in Sterically Strained Porphyrins: A Crystallographic Study of Five- and Six-coordinated Metal Complexes of 2,3,7,8,12,13,17,18-Octaethyl-5,10,15,20-tetranitroporphyrin. *J. Porphyrins Phthalocyanines* **1998,** *2*, 107–121.

14. Gibbons, D.; Flanagan, K. J.; Pounot, L.; Senge, M. O., Structure and conformation of photosynthetic pigments and related compounds. 15. Conformational analysis of chlorophyll derivatives – implications for hydroporphyrins in vivo. *Photochem. Photobiol. Sci.* **2019,** *18*, 1479–1494.

15. Roucan, M.; Flanagan, K. J.; O'Brien, J.; Senge, M. O., Nonplanar Porphyrins by *N*-Substitution: A Neglected Pathway. *Eur. J. Org. Chem.* **2018**, 6432–6446.

16. Senge, M. O., A Conformational Study of 5,10,15,20-Tetraalkyl-22H^+,24H^+-porphyrindiium Salts (Dication Salts). *Z. Naturforsch.* **2000,** *55B*, 336–344.

17. Wijesekera, T. P.; Paine, J. B., III; Dolphin, D.; Einstein, F. W. B.; Jones, T., Enforced Deformation of Porphyrins by Short-Strap Bridging. *J. Am. Chem. Soc.* **1983,** *105*, 6747–6749.

18. Chatterjee, T.; Shetti, V. S.; Sharma, R.; Ravikanth, M., Heteroatom-Containing Porphyrin Analogues. *Chem. Rev.* **2017,** *117*, 3254–3328.

19. Kielmann, M.; Grover, N.; Kalisch, W. W.; Senge, M. O., Incremental Introduction of Organocatalytic Activity into Conformationally Engineered Porphyrins. *Eur. J. Org. Chem.* **2019**, 2448–2452.

20. Senge, M. O.; Gerstung, V.; Ruhlandt-Senge, K.; Runge, S.; Lehmann, I., Non-planar porphyrins with mixed substituent pattern: bromination and formylation of ethyl-substituted tetraphenylporphyrins and tetraalkylporphyrins. *J. Chem. Soc., Dalton Trans.* **1998**, 4187–4200.

21. Lindsey, J. S., Synthetic Routes to *meso*-Patterned Porphyrins. *Acc. Chem. Res.* **2010,** *43*, 300–311.

22. Senge, M. O.; Shaker, Y. M.; Pintea, M.; Ryppa, C.; Hatscher, S. S.; Ryan, A.; Sergeeva, Y., Synthesis of *meso*-Substituted ABCD-Type Porphyrins by Functionalization Reactions. *Eur. J. Org. Chem.* **2010**, 237–258.

23. Senge, M. O., Nucleophilic Substitution as a Tool for the Synthesis of Unsymmetrical Porphyrins. *Acc. Chem. Res.* **2005,** *38*, 733–743.

24. Kalisch, W. W.; Senge, M. O., Facile *meso* Functionalization of Porphyrins by Nucleophilic Substitution with Organolithium Reagents. *Angew. Chem. Int. Ed.* **1998,** *37*, 1107–1109.

25. Kielmann, M.; Flanagan, K. J.; Norvaiša, K.; Intrieri, D.; Senge, M. O., Synthesis of a Family of Highly Substituted Porphyrin Thioethers via Nitro Displacement in 2,3,7,8,12,13,17,18-Octaethyl-5,10,15,20-tetranitroporphyrin. *J. Org. Chem.* **2017,** *82*, 5122–5134.

26. Alghooneh, L.; Eskandari, M.; Zakavi, S.; Omidyan, R., Optical properties of *β*-brominated meso-tetraphenylporphyrins: Comparative experimental and computational studies. *J. Porphyrins Phthalocyanines* **2018,** *22*, 646–657.

27. Sahoo, D.; Quesne, M. G.; de Visser, S. P.; Rath, S. P., Hydrogen-Bonding Interactions Trigger a Spin-Flip in Iron(III) Porphyrin Complexes. *Angew. Chem. Int. Ed.* **2015,** *54*, 4796–4800.

28. Piangiolino, C.; Gallo, E.; Caselli, A.; Fantauzzi, S.; Ragaini, F.; Cenini, S., The [Ru(CO)(porphyrin)]-Catalyzed Synthesis of *N*-Aryl-2-vinylaziridines. *Eur. J. Org. Chem.* **2007**, 743–750.

29. Sagun, E. I.; Zen'kevich, É. I.; Knyukshto, V. N.; Shul'ga, A. M., Spectral Manifestations of d–π Exchange and Charge Transfer Interactions in Cu(II) Porphyrins. *Opt. Spectrosc.* **2005,** *99*, 731–743.

30. Liu, T.-F.; Feng, D.; Chen, Y.-P.; Zou, L.; Bosch, M.; Yuan, S.; Wei, Z.; Fordham, S.; Wang, K.; Zhou, H.-C., Topology-Guided Design and Syntheses of Highly Stable Mesoporous Porphyrinic Zirconium Metal–Organic Frameworks with High Surface Area. *J. Am. Chem. Soc.* **2015,** *137*, 413–419.

31. Fang, Y.; Senge, M. O.; Van Caemelbecke, E.; Smith, K. M.; Medforth, C. J.; Zhang, M.; Kadish, K. M., Impact of Substituents and Nonplanarity on Nickel and Copper Porphyrin

Electrochemistry: First Observation of a Cu^{II}/Cu^{III} Reaction in Nonaqueous Media. *Inorg. Chem.* **2014,** *53*, 10772–10778.

32. Byrn, M. P.; Curtis, C. J.; Goldberg, I.; Hsiou, Y.; Khan, S. I.; Sawin, P. A.; Tendick, S. K.; Strouse, C. E., Porphyrin Sponges: Structural Systematics of the Host Lattice. *J. Am. Chem. Soc.* **1991,** *113*, 6549–6557.

33. Diskin-Posner, Y.; Patra, G. K.; Goldberg, I., Crystal Engineering of 2-D and 3-D Multiporphyrin Architectures – The Versatile Topologies of Tetracarboxyphenylporphyrin-Based Materials. *Eur. J. Org. Chem.* **2001**, 2515–2523.

34. Shmilovits, M.; Diskin-Posner, Y.; Vinodu, M.; Goldberg, I., Crystal Engineering of "Porphyrin Sieves" Based on Coordination Polymers of Pd- and Pt-tetra(4-carboxyphenyl)porphyrin. *Cryst. Growth Des.* **2003,** *3*, 855–863.

35. Diskin-Posner, Y.; Dahal, S.; Goldberg, I., Crystal Engineering of Metalloporphyrin Zeolite Analogues. *Angew. Chem. Int. Ed.* **2000,** *39*, 1288–1292.

36. Goldberg, I., Crystal engineering of nanoporous architectures and chiral porphyrin assemblies. *CrystEngComm* **2008,** *10*, 637–645.

37. Goldberg, I., Crystal engineering of porphyrin framework solids. *Chem. Commun.* **2005**, 1243–1254.

38. Titi, H. M.; Patra, R.; Goldberg, I., Exploring Supramolecular Self-Assembly of Tetraarylporphyrins by Halogen Bonding: Crystal Engineering with Diversely Functionalized Six-Coordinate $Tin(L)_2$-Porphyrin Tectons. *Chem. Eur. J.* **2013,** *19*, 14941–14949.

39. Karmakar, A.; Goldberg, I., Flexible porphyrin tetracarboxylic acids for crystal engineering. *CrystEngComm* **2010,** *12*, 4095–4100.

40. Diskin-Posner, Y.; Krishna Kumar, R.; Goldberg, I., Solid-state supramolecular chemistry of porphyrins. Stacked and layered heterogeneous aggregation modes of tetraarylporphyrins with crown ethers. *New J. Chem.* **1999,** *23*, 885–890.

41. Lipstman, S.; Goldberg, I., Supramolecular Crystal Chemistry with Porphyrin Tinkertoys. Hydrogen-Bonding and Coordination Networks with the "Chair" and "Table" Conformers of Tetra(3-carboxyphenyl)porphyrin. *Cryst. Growth Des.* **2013,** *13*, 942–952.

42. Lipstman, S.; Goldberg, I., Versatile Molecular Recognition Features of Tetra(3-pyridyl)porphyrin in Crystal Engineering. *Cryst. Growth Des.* **2010,** *10*, 4596–4606.

43. Lipstman, S.; Goldberg, I., Versatile supramolecular reactivity of zinc-tetra(4-pyridyl)porphyrin in crystalline solids: polymeric grids with zinc dichloride and hydrogen-bonded networks with mellitic acid. *Beilstein J. Org. Chem.* **2009,** *5*, 10.3762/bjoc.5.77.

44. Goldberg, I., Metalloporphyrin Molecular Sieves. *Chem. Eur. J.* **2000,** *6*, 3863–3870.

45. Patra, R.; Titi, H. M.; Goldberg, I., Crystal Engineering of Molecular Networks: Tailoring Hydrogen-Bonding Self-Assembly of Tin-Tetrapyridylporphyrins with Multidentate Carboxylic Acids As Axial Ligands. *Cryst. Growth Des.* **2013,** *13*, 1342–1349.

46. Gilday, L. C.; White, N. G.; Beer, P. D., Triazole- and triazolium-containing porphyrin-cages for optical anion sensing. *Dalton Trans.* **2012,** *41*, 7092–7097.

47. Senge, M. O.; Ema, T.; Smith, K. M., Crystal Structure of a Remarkably Ruffled Nonplanar Porphyrin (Pyridine)[5,10,15,20-Tetra(tert-butyl)porphyrinato]zinc(II). *J. Chem. Soc., Chem. Commun.* **1995**, 733–734.

48. Senge, M. O.; Kalisch, W. W.; Bischoff, I., The Reaction of Porphyrins with Organolithium Reagents. *Chem. Eur. J.* **2000,** *6*, 2721–2738.

49. Senge, M. O.; Kalisch, W. W.; Runge, S., *N*-Methyl Derivatives of Highly Substituted Porphyrins – The Combined Influence of both Core and Peripheral Substitution on the Porphyrin Conformation. *Liebigs Ann. Recl.* **1997**, 1345–1352.

50. Senge, M. O., On the Molecular Stereochemistry of the 21,22,23-trimethyl-5,10,15,20-Tetraphenylporphyrin Cation. *J. Porphyrins Phthalocyanines* **1999,** *3*, 216–223.

51. Senge, M. O.; Forsyth, T. P.; Nguyen, L. T.; Smith, K. M., Sterically Strained Porphyrins—Influence of Core Protonation and Peripheral Substitution on the Conformation of Tetra-meso-, Octa-β-, and Dodeca-Substituted Porphyrin Dications. *Angew. Chem. Int. Ed.* **1995,** *33*, 2485–2487.

52. Senge, M. O.; Richter, J.; Bischoff, I.; Ryan, A., Highly substituted 2,3,7,8,12,13,17,18-octaethylporphyrins with *meso* aryl residues. *Tetrahedron* **2010,** *66*, 3508–3524.

53. Ghiassi, K. B.; Powers, X. B.; Wescott, J.; Balch, A. L.; Olmstead, M. M., Crystal Engineering Gone Awry. What a Difference a Few Methyl Groups Make in Fullerene/Porphyrin Cocrystallization. *Cryst. Growth Des.* **2016,** *16*, 447–455.

54. Hope, H., X-Ray Crystallography: A Fast, First-Resort Analytical Tool. *Prog. Inorg. Chem.* **2007**, 1–19.

55. *Saint*, Version 8.37a; Bruker AXS, Inc.: Madison, WI, 2013.

56. *SADABS*, version 2016/2; Bruker AXS, Inc.: Madison, WI, 2014.

57. *APEX3*, Version 2016.9-0; Bruker AXS, Inc.: Madison, WI, 2016.

58. Dolomanov, O. V.; Bourhis, L. J.; Gildea, R. J.; Howard, J. A. K.; Puschmann, H., OLEX2: a complete structure solution, refinement and analysis program. *J. Appl. Crystallogr.* **2009,** *42*, 339–341.

59. Sheldrick, G., SHELXT - Integrated space-group and crystal-structure determination. *Acta Cryst. Sect. A* **2015,** *71*, 3–8.

60. Jentzen, W.; Ma, J.-G.; Shelnutt, J. A., Conservation of the Conformation of the Porphyrin Macrocycle in Hemoproteins. *Biophys. J.* **1998,** *74*, 753–763.

61. Jentzen, W.; Simpson, M. C.; Hobbs, J. D.; Song, X.; Ema, T.; Nelson, N. Y.; Medforth, C. J.; Smith, K. M.; Veyrat, M.; Mazzanti, M.; Ramasseul, R.; Marchon, J. C.; Takeuchi, T.; Goddard, W. A.; Shelnutt, J. A., Ruffling in a Series of Nickel(II) *meso*-Tetrasubstituted Porphyrins as a Model for the Conserved Ruffling of the Heme of Cytochromes *c*. *J. Am. Chem. Soc.* **1995,** *117*, 11085–11097.

62. Jentzen, W.; Song, X.-Z.; Shelnutt, J. A., Structural Characterization of Synthetic and Protein-Bound Porphyrins in Terms of the Lowest-Frequency Normal Coordinates of the Macrocycle. *J. Phys. Chem. B* **1997,** *101*, 1684–1699.

63. *NSDGUI*, Version 1.3 alpha; Sandia National Laboratory: New Mexico, 2001.

64. Turner, M. J.; McKinnon, J. J.; Wolff, S. K.; Grimwood, D. J.; Spackman, P. R.; Jayatilaka, D.; Spackman, M. A. *CrystalExplorer17*, Version 17.5; University of Western Australia, 2017.

65. Spackman, M. A.; Jayatilaka, D., Hirshfeld surface analysis. *CrystEngComm* **2009,** *11*, 19–32.

66. Lindsey, J. S.; Hsu, H. C.; Schreiman, I. C., Synthesis of Tetraphenylporphyrins Under Very Mild Conditions. *Tetrahedron Lett.* **1986,** *27*, 4969–4970.

67. Schindler, J.; Kupfer, S.; Ryan, A. A.; Flanagan, K. J.; Senge, M. O.; Dietzek, B., Sterically induced distortions of nickel(II) porphyrins – Comprehensive investigation by

DFT calculations and resonance Raman spectroscopy. *Coord. Chem. Rev.* **2018,** *360*, 1–16.

68. Hoshino, A.; Ohgo, Y.; Nakamura, M., Synthesis and inversion barriers of undeca- and dodeca-substituted saddle shaped porphyrin complexes. *Tetrahedron Lett.* **2005,** *46*, 4961–4964.

69. Adler, A. D.; Longo, F. R.; Kampas, F.; Kim, J., On the preparation of metalloporphyrins. *J. Inorg. Nucl. Chem.* **1970,** *32*, 2443–2445.

70. Dumoulin, F.; Ahsen, V., Click chemistry: the emerging role of the azide-alkyne Huisgen dipolar addition in the preparation of substituted tetrapyrrolic derivatives. *J. Porphyrins Phthalocyanines* **2011,** *15*, 481–504.

71. Grimes, K. D.; Gupte, A.; Aldrich, C. C., Copper(II)-Catalyzed Conversion of Aryl/Heteroaryl Boronic Acids, Boronates, and Trifluoroborates into the Corresponding Azides: Substrate Scope and Limitations. *Synthesis* **2010**, 1441–1448.

72. Medforth, C. J.; Senge, M. O.; Smith, K. M.; Sparks, L. D.; Shelnutt, J. A., Nonplanar Distortion Modes for Highly Substituted Porphyrins. *J. Am. Chem. Soc.* **1992,** *114*, 9859–9869.

73. Senge, M. O.; Kalisch, W. W., Synthesis and Structural Characterization of Nonplanar Tetraphenylporphyrins and Their Metal Complexes with Graded Degrees of *β*-Ethyl Substitution. *Inorg. Chem.* **1997,** *36*, 6103–6116.

74. Sparks, L. D.; Medforth, C. J.; Park, M. S.; Chamberlain, J. R.; Ondrias, M. R.; Senge, M. O.; Smith, K. M.; Shelnutt, J. A., Metal dependence of the nonplanar distortion of octaalkyltetraphenylporphyrins. *J. Am. Chem. Soc.* **1993,** *115*, 581–592.

For Table of Contents Only
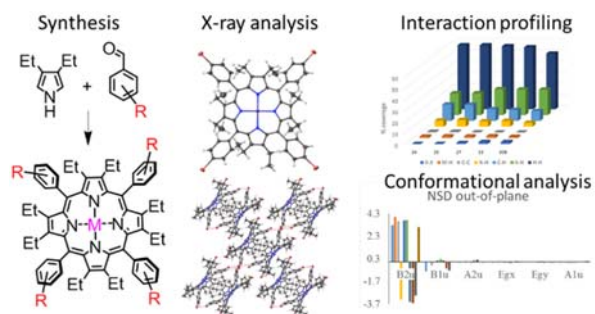
SYNOPSIS

Herein we describe the synthesis of several new 5,10,15,20-tetraaryl-(X)-substituted-2,3,7,8,12,13,17,18-octaethylporphyrins (where X is a halogen, nitrogenous, alkyne, benzyloxy group, or triazole-linked benzene group with a *para*-functionalized moiety) and their metal(II) counterparts. Using X-ray diffraction we have highlighted how the interaction profiles and packing arrangements are affected by the substituent used, metal(II) center, or solvent inclusion, and how these observations can indicate the potential to create selective and functional receptor sites based on free base porphyrins.